Robustness assessment of reinforced concrete structures for different failure scenarios

(Article begins on next page)

01 October 2025

ROBUSTNESS ASSESSMENT OF REINFORCED CONCRETE STRUCTURES FOR DIFFERENT FAILURE SCENARIOS

E. Miceli[1], M. De Iuliis[2], P. Castaldo[3]

[1] Department of Structural, Geotechnical and Building Engineering (DISEG), Politecnico di Torino, Turin, Italy (corresponding author), e-mail: elena.miceli@polito.it

[2] Department of Structural, Geotechnical and Building Engineering (DISEG), Politecnico di Torino, Turin, Italy, e-mail: massimiliano.deiuliis@polito.it

[3] Department of Structural, Geotechnical and Building Engineering (DISEG), Politecnico di Torino, Turin, Italy, e-mail: paolo.castaldo@polito.it ; pcastaldo@unisa.it

Corresponding Author

Elena Miceli

elena.miceli@polito.it

+39 0110905305

ROBUSTNESS ASSESSMENT OF REINFORCED CONCRETE STRUCTURES FOR DIFFERENT FAILURE SCENARIOS

E. Miceli[1], M. De Iuliis[2], P. Castaldo[3]

[1] Department of Structural, Geotechnical and Building Engineering (DISEG), Politecnico di Torino, Turin, Italy (corresponding author), e-mail: elena.miceli@polito.it

[2] Department of Structural, Geotechnical and Building Engineering (DISEG), Politecnico di Torino, Turin, Italy, e-mail: massimiliano.deiuliis@polito.it

[2] Department of Structural, Geotechnical and Building Engineering (DISEG), Politecnico di Torino, Turin, Italy, e-mail: paolo.castaldo@polito.it ; pcastaldo@unisa.it

ABSTRACT

This study describes the robustness assessment of 3D reinforced concrete structures analyzing the response of the 2D frames in different design configurations and failure scenarios. The structures are characterized by both frames with wide beams and seismic-resistant frames with deep beams. Three structural design configurations are investigated: the code configuration and two configurations improved with respect to robustness. For any configuration, four different failure scenarios are considered, removing specific supporting columns. For any failure scenario and design configuration, 2D non-linear finite element (NLFE) simulations are carried out to evaluate the behavior of the two frames along the two orthogonal directions. In any analysis, the contribution of the frame, located along the orthogonal direction, is considered by means of translation springs having non-linear constitute laws specific for the inward and outward movements. By imposing an increasing displacement at the top of the removed column, the corresponding capacity curves have been defined. Successively, the two plane NLFE capacity curves are superimposed to define the global response of the framed structure. This superposition is validated through the comparison with 3D non-linear analyses. The results demonstrate the importance to calibrate the non-linear constitutive laws of the springs, particularly, for large vertical displacements and some failure scenarios. The frames with wide beams improve, especially, the global ductility. In addition, it is confirmed the superposition of the plane NLFE capacity curves of the two orthogonal frames. Finally, by means of the energy-based approach, the benefits of the robustness design improvements are highlighted.

Keywords: structural robustness, design/structural configuration, 2D NLFE simulation, global capacity curve, superposition, 3D model, reinforced concrete, failure scenarios, non-linear springs.

1. INTRODUCTION

Nowadays, the scientific community is facing the need to take into account design scenarios which were not considered in the past, like the extreme events. An extreme event is a situation that is very unlikely to occur but has catastrophic consequences in terms of economic losses, fatalities and injuries [1]. Structural robustness is a key concept as it represents the response that systems must provide in the occurrence of an extreme event or, in other words, to avoid phenomena of disproportionate or progressive collapse [2]. One of the most widespread methods to evaluate the structural robustness of a reinforced concrete (RC) building is to study the alternative load path (i.e., ALP analysis) by removing a supporting column, as suggested by codes and guidelines [3]-[7]. Both membrane (in case of full slab elements) or catenary (in case of beam elements) mechanisms are crucial aspects to investigate since they guarantee a certain degree of bearing capacity in case of removal of a supporting column. For instance, in [8], the reliability of planar RC frames under column loss scenario is studied,

accounting, in a simplified way, for the developed membrane actions between directly and indirectly affected elements. A numerical validation on three real-scale RC beam-column-slab sub-assemblies was developed in [9], in order to study the parameters influencing the activation of tensile membrane actions (i.e., constraint conditions, slab thickness, reinforcement ratio). Seismic and progressive collapse assessments on an RC framed structure was carried out in [10], in order to investigate the effectiveness of retrofit interventions. The experimental study on RC slab strips under shear and tensile loads was numerically studied in [11], to assess structural robustness enhancements due to the activation of membrane effects. In fact, the cracks, generated at the extrados of a continuous RC floor close to a column accidentally lost, generate a constraint condition to the radial expansion and, thus, membrane forces which increase the load bearing capacity of the system [12]-[15]. However, most of these results consider full slabs having a thickness of more than 15-20 cm. This three-dimensionality is not only guaranteed by the slab but also by the frames in the orthogonal directions [16]. For example, the importance of including transverse frames in a model of progressive collapse scenario is demonstrated by a numerical comparison between 2D and 3D analyses in [17]-[18]. This conclusion was also reached by means of an experimental analysis on progressive collapse resistance of beam-column subassemblies considering transverse beam effects [19]. Specifically, it was demonstrated that the capacity curve for a cross-beam subassembly was almost coincided with the superposition of that for the longitudinal beam and transverse beam. An experimental and numerical study on the progressive collapse for three-dimensional RC structures is conducted in [20], proposing analytical models to include the effect of secondary beams and torsion of primary ones. The experimental results in [21] demonstrated that 3D effects, excluding the slab, can increase the bearing capacity of the frame of more than 100%. Similar conclusions were drawn by [22], with a numerical comparison between planar systems and 3D models. This issue can be very relevant for buildings having slabs with one-way joists (typical, e.g., in Italy). However, 3D analyses, especially in dynamic field, are not always the preferable choice since require large computational efforts and expertise.

As for, particularly, structures having slabs with one-way joists, this study proposes to include some relevant three-dimensional effects by investigating the bearing capacity of the two orthogonal planar frames directly involved in the column removal scenario. Hence, a large parametric analysis is carried out to assess the robustness of 3D ordinary RC moment resisting (MR) structures analyzing the response of the planar frames along the two orthogonal directions. The 3D structure is located in a highly seismic zone and characterized by both frames with wide beams and seismic-resistant frames with deep beams, designed according to both Italian [23] and European [24] codes. Specifically, inspired by [25]-[26], three structures corresponding to three design configurations are investigated: the *STANDARD* one according to the codes is compared with the configuration having continuous, symmetrical and equal beam longitudinal reinforcement in all the floors in addition to side face rebars (denoted as *CSE+rebars*) and, then, with the configuration where the symmetry and floor equality are excluded (denoted as *C+rebars*). For all the three design configurations, four different failure scenarios are considered by removing specific supporting columns. For any specific failure scenario and design configuration, 2D non-linear finite element (NLFE) pushdown simulations are carried out to evaluate the behavior of the two RC frames along the two orthogonal directions. In any 2D simulation, the contribution of the orthogonal frame is taken into account by means of translation springs having non-linear constitute laws properly calibrated along both inward and outward directions. By imposing an increasing displacement at the top of the removed column, the corresponding capacity curves are defined. Successively, these plane NLFE capacity curves are superimposed to achieve the global response of the structures. This superposition is validated through the comparison with corresponding 3D non-linear capacity curves. The results demonstrate the importance to calibrate the non-linear constitutive laws of the springs, especially, for large vertical displacements and some failure scenarios when buildings have also wide beams. In fact, frames with wide beams provide a contribution, especially, in terms of ductility. Moreover, the results validate the superposition of the plane NLFE capacity curves of the two orthogonal frames, involved in the same failure scenario, to define the global capacity curves for both the different design configurations

and failure scenarios. Finally, the energetic equivalence approach [27] allowed to assess the effectiveness of the design improvements in the plane frames to enhance the robustness of the 3D structures against the different failure scenarios.

2. ROBUSTNESS OF RC STRUCTURES: ANALYSIS AND PROPOSALS

The structural behavior of RC frames in case of a column loss scenario has been widely studied by means of experimental tests on beam-column subassemblies [28]-[31]. This response, expressed in terms of capacity curve (i.e., load-displacement curve), presents three phases: i) the first phase (i.e., *flexural-arching phase*) governed by the bending of the beams with outward horizontal displacements of the beam-column nodes caused by compressive axial forces in the beams; this phase ends when the resistance peak is reached, denoted herein as $P_{MAX,FL}$; ii) the second phase (i.e., *softening phase*) where a softening response occurs with a reduction of the horizontal displacements and of the reaction in the point of column removal due to the crushing of concrete; iii) the third phase (i.e., *catenary effect*) having an increase of the reaction for higher vertical displacement in the point of removal with inward horizontal displacements of beam-column nodes; this phase ends with the collapse or ultimate peak, identified as $P_{MAX,ULT}$, and is governed by the response of the longitudinal reinforcement.

Note that a relevant influence of the axial compression force in the beams can occur mainly in the first and, also in the second phase.

According to the energetic approach by [27], the capacity curve is useful to define the internal work U_i (i.e., the energy adsorbed by the structure when a column is removed), whereas the external work W_{ext} (i.e., the work done by the gravity loads) is provided by the corresponding reaction P_{EXT} of the column before the removal. This reaction is computed within the accidental combination of the external loads (i.e., permanent structural loads, non-structural loads and variable loads) according to the codes [23],[24]. The performance point (i.e., point of dynamic equilibrium) is, then, evaluated in correspondence of the equality between the external work and internal energy.

As for the frames of RC systems, different literature studies and codes have provided the following provisions to improve the robustness behaviour:

- **Symmetry (S):** the recommendation provided by codes and literature studies (e.g., [7],[32]) consists in arranging the same reinforcement in the two chords of the beam, making the section symmetrical;
- **Support-continuity:** if the longitudinal reinforcement bars are continuous over the supports, they are useful to favour the tie behavior of the beams [4]-[6],[33]-[35];
- **Equivalent elastic lateral springs:** the presence of the orthogonal structural systems can highly and positively influence the response of the structure when a supporting column collapses, as demonstrated in [12],[16]-[19],[36]. As observed in [25], the implementation of equivalent horizontal elastic springs influences significantly the activation of the catenary behavior;
- **Floor equality (E):** it is suggested to apply to all the floors the same amount of reinforcement of the first floor (i.e., the largest one) to achieve a Vierendeel behavior [25];
- **Continuity (C):** it is essential to have the longitudinal reinforcement bars continuous over the supports and along the beams (i.e., not less than 30% of the span length) in addition to the anchorage length at each edge of the beams, especially, in the upper chord of the beams, as proposed in [25];
- **Side face rebars:** the side face reinforcement bars determine important improvements. In fact, as proposed in [25], they are crucial to anticipate the transition towards the catenary activation at vertical displacements lower than the depth of the beam cross-section.

These modifications of the longitudinal reinforcement influence the seismic design with respect to the capacity design principles and a cyclic redesign of Ultimate and Serviceability Limit States (U-SLSs) as well as seismic verifications is, thus, necessary, as discussed in [25].

In this study, the following additional issues, useful to both design and analysis with respect to the robustness response, are investigated:

- **Non-linear lateral springs:** the constitutive laws of the springs are properly calibrated for both

inward and outward movements to model the horizontal contribution provided by the orthogonal out-of-plane systems (i.e., beams and columns of the orthogonal out-of-plane frames). In this way, the entire development of the mechanical response of all the frames is explicitly taken into account starting from the fully elastic up to fully inelastic behavior of all the beams and columns;
- **Superposition of 2D capacity curves:** for a specific column loss, the plane non-linear responses of the two orthogonal frames directly affected by the same failure scenario are computed and, then, superimposed to achieve the global capacity curve including the corresponding 3D non-linear effects along the two directions. The validation of this superposition is performed through the comparison with the corresponding capacity curve derived from a 3D non-linear analysis.

These proposals are tested by means of a wide parametric analysis: three 3D ordinary RC MR structures, having slabs with one-way joists and composed of both wide and deep beams, corresponding to three different design configurations are examined with respect to four failure scenarios. In detail, the *STANDARD* code design configuration is compared with the structural configuration having all the previous recommendations (i.e., *CSE+rebars*) and, then, with the design configuration without the symmetry and floor equality (i.e., *C+rebars*). In the following, the three design configurations are analyzed by means of 2D NLFE models for four failure scenarios of interest to the robustness issue.

3. DIFFERENT DESIGN CONFIGURATIONS FOR 3D STRUCTURES IN SEISMIC ZONE

This section deals with the design of the three 3D structures corresponding to three design configurations to test the proposals.

The first structural configuration denoted as *STANDARD* design refers to a 3D ordinary building, composed of multi-story RC MR frames, with an inter-story height of 3.5 m, regular in elevation and symmetrical in both directions. The plan of the building, illustrated in Fig. 1, has four spans in x-direction and three in y-direction with a span length of 5 m in both directions. Additionally, the dashed lines in Fig. 1 indicate the wide beams in parallel to the direction of the one-way slab's joists, while the continuous lines indicate the deep beams. In this work, wide beams indicate beams having the same depth of the slab including the joists, while deep beams are higher than the height of the slab and joists. Therefore, the RC system has 2D frames with different geometries and resisting characteristics to be representative of a generic case study. Furthermore, Fig. 1 indicates the studied failure scenarios representative of the possible local damages that can trigger a progressive collapse.
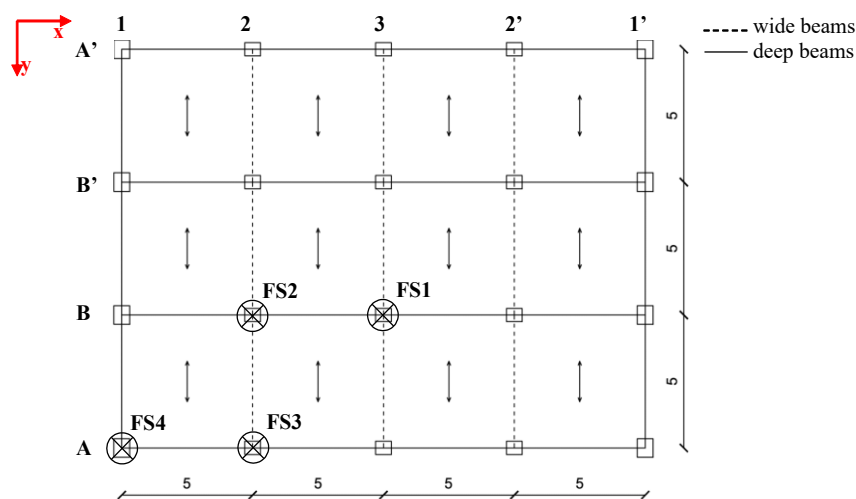

Fig. 1 Plan view together with failure scenarios (FSs) and direction of the slab's joists. Measurements in m.

The *STANDARD* design is carried out combining gravity loads with snow and wind actions according to [3] and [23] as well as following the seismic design guidelines of both NTC2018 [23] and EC8 [24], assuming L'Aquila city (Italy) as reference site and a high ductility class. It is important to underline that the deep beams belong to the seismic-resistant frames, while the other frames with

wide beams are designed as secondary structural elements according to [23]-[24]. A large height of the beam in the MR frames has been selected in order to enhance the bearing capacity of the frame in line with [30]. At the same time, a relatively large height-to-width ratio (i.e., 80%) can be beneficial to increase the flexural-arching response as well as to facilitate a more ductile behavior for the catenary [37]. In all structural elements, C25/30 concrete [23] is used, adopting a 3.5 cm concrete clear cover. For both longitudinal and transversal reinforcement, B450C steel bars [23] are employed as follows: ϕ18 for the longitudinal reinforcement of the deep beams, ϕ14 for the longitudinal reinforcement of the wide beams, ϕ20 for the columns and ϕ8 for the stirrups. In all the beam-column nodes, ϕ8 stirrups are placed with a spacing of 50 mm. The stirrup spacing varies as a function of the extension of the dissipative zones (Table 1): the dissipative zones of the beams have an extension of 1m, while the dissipative zone for the column is set to 0.6m, in accordance with the construction details [23]-[24]. Structural and modal analysis together with seismic verifications for the different combinations [3],[23],[24] are implemented in the numerical code SAP2000 [38]. The structural detailing of columns, beams and nodes derives from the verifications of the ULSs and SLSs as well as of capacity-design principles as per the various seismic code LSs [23]-[24]. The section properties of columns, beams and nodes for this first design configuration are detailed in Table 1.

Table 1. Section proprieties of the RC elements in the *STANDARD* configuration.

Element	Plan location	Floor	Size [mm²]	Longitudinal bars *	Stirrups *
Beams	A1-A1'	1ˢᵗ-3ʳᵈ	400x500	4 ϕ_u18 + 3 ϕ_l18 (D), 2 ϕ_u 18 + 3ϕ_l18 (ND)	2-leg ϕ8/100 (D), 150(ND)
		4ᵗʰ-5ᵗʰ	400x500	3 ϕ_u18 + 3 ϕ_l18 (D), 2 ϕ_u 18 + 3ϕ_l18 (ND)	2-leg ϕ8/100 (D), 150(ND)
	B1-B1'	1ˢᵗ-3ʳᵈ	400x500	5 ϕ_u18 + 3 ϕ_l18 (D), 2 ϕ_u 18 + 3ϕ_l18 (ND)	2-leg ϕ8/100 (D), 150(ND)
		4ᵗʰ-5ᵗʰ	400x500	4 ϕ_u18 + 3 ϕ_l18 (D), 2 ϕ_u 18 + 3ϕ_l18 (ND)	2-leg ϕ8/100 (D), 150(ND)
	A2-A'2 A3-A'3	1ˢᵗ-5ᵗʰ	230x600	2ϕ_u14 + 2ϕ_l14	2-leg ϕ8/100
Columns	A1, B1	all	600x500	10 ϕ20	4-leg ϕ8/100 (D), 150(ND)
	A2, A3, B2, B3	all	600x700	16 ϕ20	4-leg ϕ8/100 (D), 150(ND)
Nodes	all	all			4-leg ϕ8/50

*D indicates the dissipative zone of the resisting element while ND the non-dissipative zone; ϕ_u and ϕ_l are, respectively, the longitudinal reinforcement in the upper and lower chords.

Table 2. Section proprieties of the RC elements in the *C+rebars* configuration.

Element	Plan location	Floor level	Size [mm²]	Longitudinal bars *	Stirrups *
Beams	A1-A1'	1ˢᵗ-3ʳᵈ	400x500	4 ϕ_u18 + 3 ϕ_l18 + 4 ϕ_s16	2-leg ϕ8/ 75 (D), 150(ND)
		4ᵗʰ-5ᵗʰ	400x500	3 ϕ_u18 + 3 ϕ_l18 + 4 ϕ_s16	2-leg ϕ8/ 75 (D), 150(ND)
	B1-B1'	1ˢᵗ-3ʳᵈ	400x500	5 ϕ_u18 + 3 ϕ_l18 + 4 ϕ_s16	2-leg ϕ8/ 75 (D), 150(ND)
		4ᵗʰ-5ᵗʰ	400x500	4 ϕ_u18 + 3 ϕ_l18 + 4 ϕ_s16	2-leg ϕ8/ 75 (D), 150(ND)
	A2-A'2 A3-A'3	1ˢᵗ-5ᵗʰ	230x600	2 ϕ_u14 + 2 ϕ_l14	2-leg ϕ8/100
Columns	A1, B1	all	600x500	10 ϕ20	4-leg ϕ8/ 100 (D), 150(ND)
	A2, A3, B2, B3	all	600x700	16 ϕ20	4-leg ϕ8/ 100 (D), 150(ND)
Nodes	all	all			4-leg ϕ8/ 50

*D indicates the dissipative zone of the resisting element while ND the non-dissipative zone; ϕ_u and ϕ_l are, respectively, the longitudinal reinforcement in the upper and lower chords and ϕ_s indicate side face rebars

As for the second design configuration denoted as *"C+rebars"* configuration, the design suggestions of the continuity of the beam longitudinal reinforcement together with the presence of the side face rebars are considered. The additional rebars are two levels of 2ϕ16 located at around 1/3 and 2/3 of the beam height. The extra reinforcements are placed continuously along the length of each beam across all five floors. The presence of the side face rebars, after the verification for the ULSs, SLSs

and seismic LSs, leads to a change in the stirrups step in the dissipative areas of the seismic-resistant beams for all the floors from 10 cm to 7.5 cm. The new section reinforcement characteristics are presented in Table 2.

Regarding the third structural configuration denoted as *"CSE+rebars"* configuration, the equal reinforcement arrangements of the floors and the symmetry of the cross-section are adopted leading to changes in the reinforcement layout of the structural elements, after the verification for ULSs, SLSs and seismic capacity design. Specifically, an increase of the stirrups diameter in the beam-column nodes of the entire building from 8 mm to 10 mm (Table 3) has been necessary.

Note that the modifications of the last two configurations are not implemented for the wide beams but only for the beams of the MR frames since the wide beams respect the continuity and symmetry principles in the "*STANDARD*" model, and do not have a sufficient space for the side face rebars.

Table 3. Section proprieties of the RC elemenents in the *CSE+rebars* configuration.

Element	Plan location	Floor level	Size [mm²]	Longitudinal bars *	Stirrups *
Beams	A1-A1'	all	400x500	$4\,\phi_u18 + 4\,\phi_l18 + 4\,\phi_s16$	2-leg ϕ8/ 75 (D), 150(ND)
	B1-B1'	all	400x500	$5\,\phi_u18 + 5\,\phi_l18 + 4\,\phi_s16$	2-leg ϕ8/ 75 (D), 150(ND)
	A2-A'2 A3-A'3	all	230x600	$2\,\phi_u14 + 2\,\phi_l14 + 4\,\phi_s16$	2-leg ϕ8/100
Columns	A1, B1	all	600x500	10 ϕ20	4-leg ϕ8/ 100 (D), 150(ND)
	A2, A3, B2, B3	all	600x700	16 ϕ20	4-leg ϕ8/ 100 (D), 150(ND)
Nodes	all	All			4-leg ϕ10/ 50

*D indicates the dissipative zone of the resisting element while ND the non-dissipative zone; ϕ_u and ϕ_l are, respectively, the longitudinal reinforcement in the upper and lower chords and ϕ_s indicate side face rebars.

4. DEFINITION OF NLFE MODELS TO SIMULATE THE FAILURE SCENARIOS

This section describes how the 2D NLFE models of the frames, involved in the failure scenarios, have been defined for each structural configuration to achieve the 2D capacity curves. In fact, 2D NLFE simulations allow to assess the non-linear response of RC frames with respect to ductile or brittle failures in local or global resistance mechanisms. On the contrary, 3D FE analyses are not considered since one of the aims of the study is to superimpose the results from plane NLFE simulations of 2D frames properly designed to improve the robustness of 3D RC structures in seismic zone. This can be very effective, especially, for structures with RC slabs having joists along only one direction to validate how the robustness suggestions have been implemented within the seismic design, particularly, of the plane MR frames. In this way, the design of 3D RC structures can be performed through the design of the plane MR frames including both seismic and robustness principles.

The numerical predictive models are performed considering the FEM software ATENA 2D [39]. All the assumptions behind the numerical modeling [40]-[48] have been validated by reproducing the results of the experimental test on a beam-column subassembly [31], whose details are given in Appendix A. Of course, the only differences concern the material properties and geometrical characteristics, while the other assumptions and modelling strategies are the same. Specifically, the compressive responses of concrete related to *STANDARD, C+rebars* and *CSE+rebars* configurations are illustrated, respectively, in Fig. 2, Fig. 3 and Fig. 4 distinguishing between the different structural elements due to the different confinement effects. In detail, the constitutive model has been formulated for: unconfined concrete (i.e., concrete effective cover - "unconfined"), concrete in non-dissipative regions of beams ("beam Non-Dissipative"), concrete in dissipative areas of beams ("beam Dissipative" considering the step of the stirrups), concrete in wide beams ("Wide beam"), concrete in non-dissipative sections of columns ("column ND"), concrete in dissipative sections of columns ("column D", considering the step of the stirrups and the two different cross sections) and concrete in beam-column nodes (considering the stirrup diameter and different section properties). Note that the confinement effects in the beams are crucial since, during the initial stage of the mechanism, the

beams are subjected to compressive arching forces which determine relevant axial compressive loads on the beams. If not considered, the capacity of the structural system would be underestimated, as demonstrated in Appendix A. However, this is valid for the scenarios where the lost column is not perimetral. For cases with a perimetral removed column, confinement effects on the beams are not accounted for and the constitutive law is that of the "unconfined" curve in Fig. 2, Fig. 3 and Fig. 4. The tensile response of concrete is depicted in Fig. 5(a) for all the three configurations, while the reinforcement stress-strain law is a bi-linear curve, equal in tension and in compression, and it is shown in Fig. 5(b). Particularly, an ultimate-to-yield strength ratio of 1.25 is set and an ultimate strain of 0.18 is assumed. These assumptions are based on many experimental tests [28]-[31],[49]-[53]. Finally, the loss of a supporting column is reproduced by imposing a vertical displacement, with steps of 1 cm, at the top point of the removed column, without considering any other action. This step-by-step procedure allows to evaluate the structural response as well as the deformation and crack pattern together with stress state, investigating the residual resistance of the structure (i.e., capacity curve). Ultimately, fully fixed constraints are set at the base of each column.
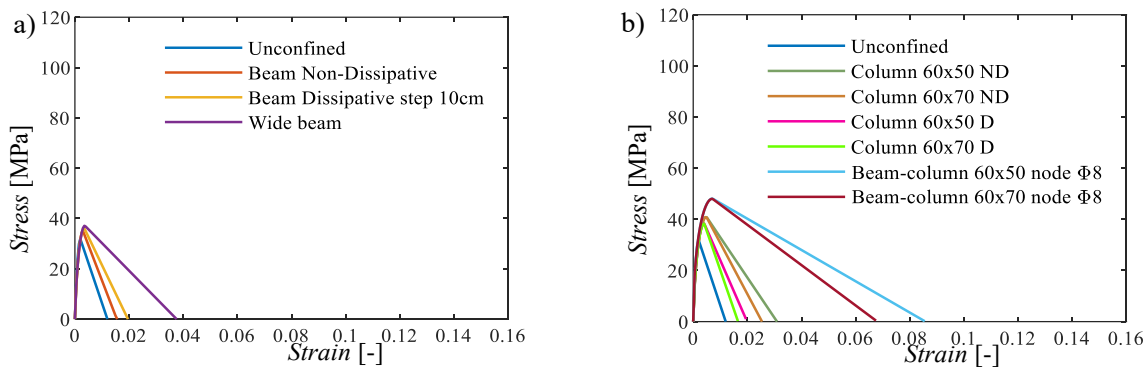

Fig. 2 Constitutive laws - "*STANDARD*" configuration: (a) concrete compressive behavior for beams; (b) concrete compressive behavior for columns. Mean values of the mechanical properties are assumed.
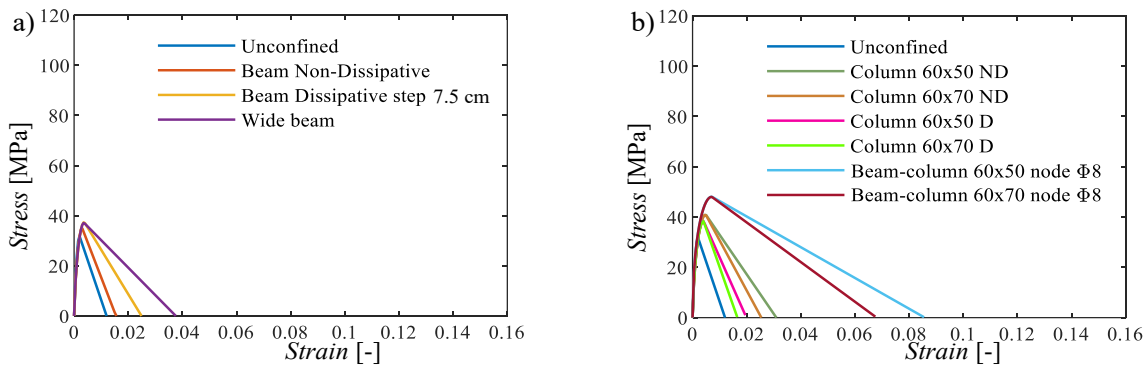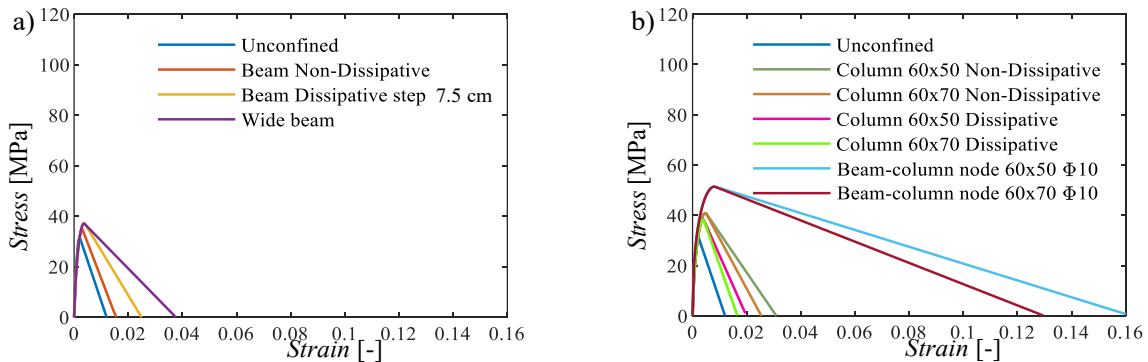

Fig. 3 Constitutive laws - "*C+rebars*" configuration: (a) concrete compressive behaviour for beams; (b) concrete compressive behavior for columns. Mean values of the mechanical properties are assumed.

Fig. 4: Constitutive laws - "*CSE+rebars*" configuration: (a) concrete compressive behaviour for beams; (b) concrete compressive behavior for columns. Mean values of the mechanical properties are assumed.
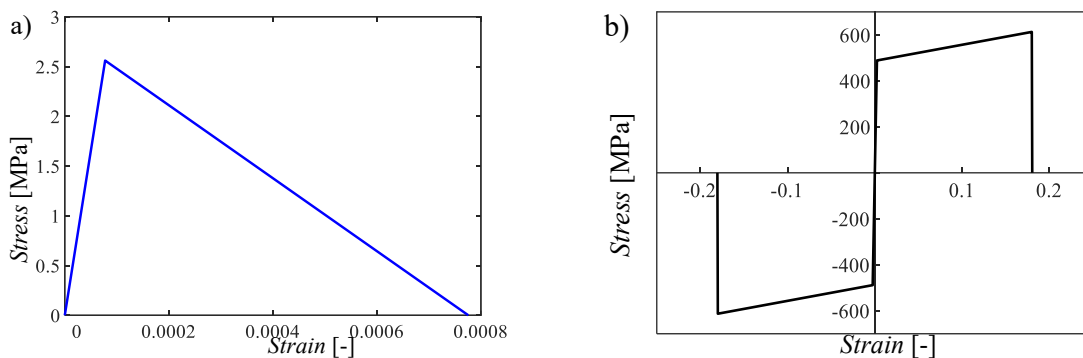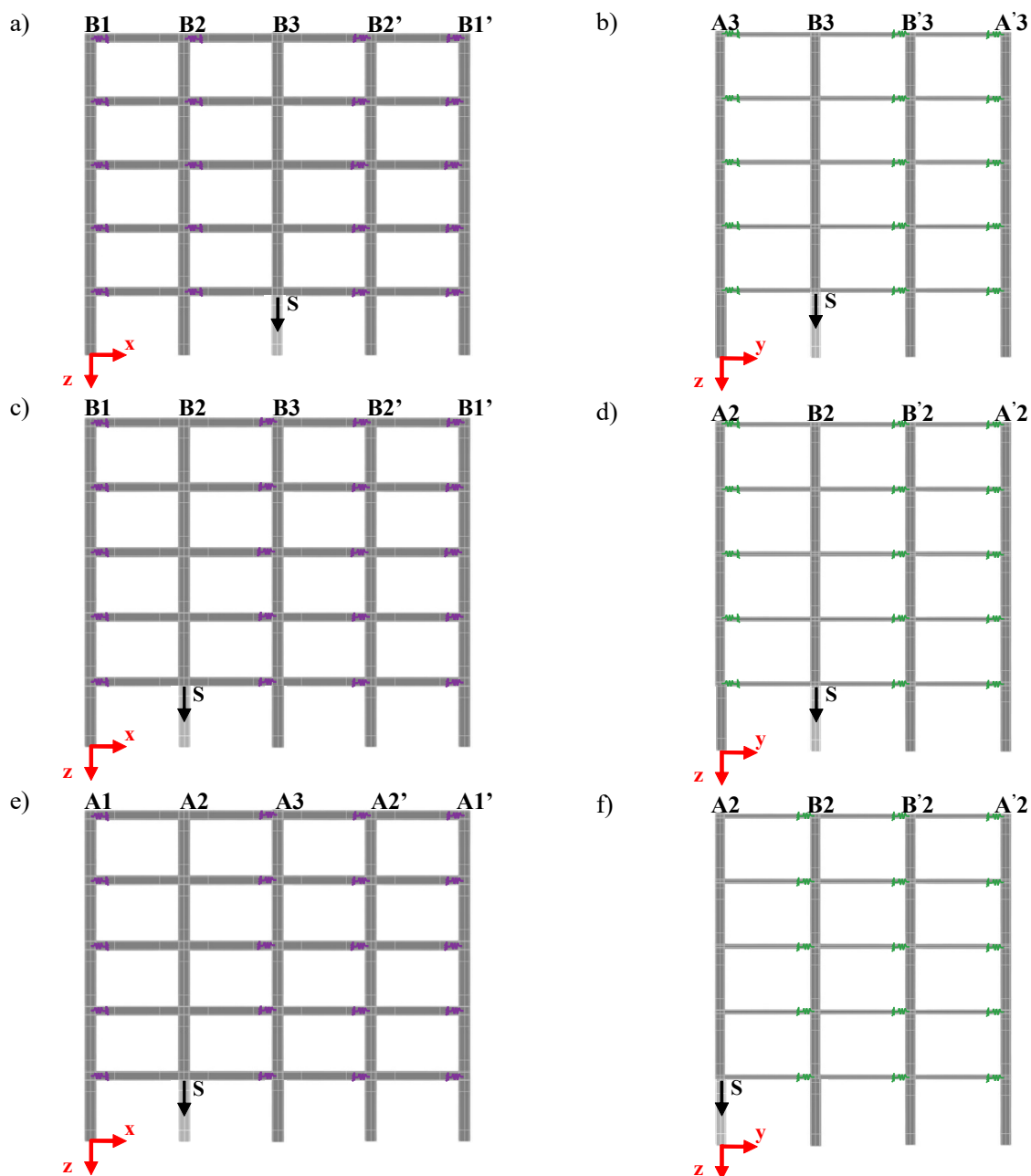
Fig. 5 Constitutive laws: (a) concrete tensile behavior; (b) steel tensile and compressive behavior. Mean values of the mechanical properties are assumed.

5. FAILURE SCENARIOS AND CALIBRATION OF THE NON-LINEAR SPRINGS

For the three structural configurations, this study explores four distinct failure scenarios, as shown in Fig. 1 and Fig. 6.
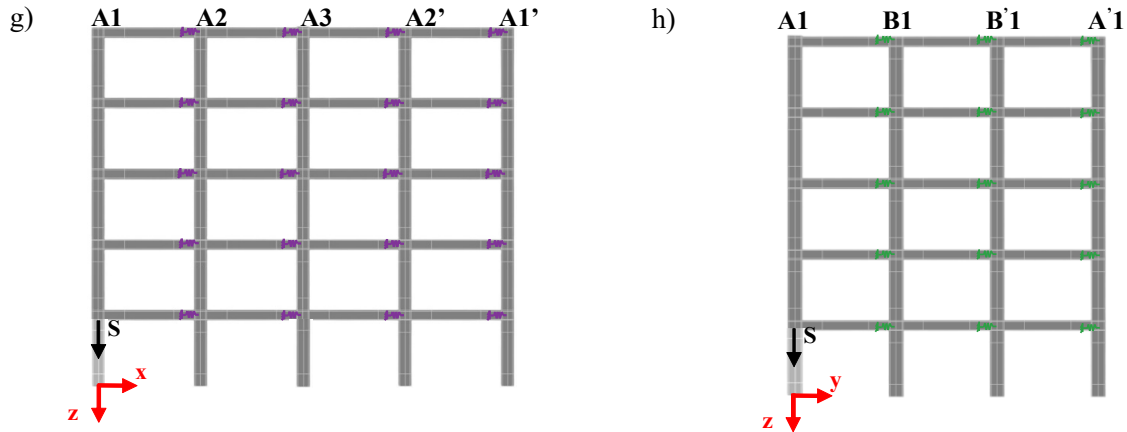
Fig. 6 The NLFE models for pushdown analyses of the frames involved in the: (a)-(b) first failure scenario-FS1; (c)-(d) second failure scenario-FS2; (e)-(f) third failure scenario-FS3; (g)-(h) fourth failure scenario-FS4. The arrow "S" denotes the imposed displacement at the top of the removed column.

These four failure scenarios represent the relevant and worst situations in the building where any contribution deriving from infills [37] is absent. The first failure scenario (FS1 - Fig. 1) involves the removal of column B3 and affects the FS1-x and FS1-y frames (Fig. 6(a)-(b)); the second (Fig. 1) involves the removal of column B2 and affects the FS2-x and FS2-y frames (Fig. 6(c)-(d)); the third (Fig. 1) involves the removal of column A2 and affects the FS3-x and FS3-y frames (Fig. 6(e)-(f)); the fourth (Fig. 1) involves the removal of column A1 and affects the FS4-x and FS4-y frames (Fig. 6(g)-(h)). In total, 24 different frames are analyzed through 2D NLFE pushdown analyses, considering the four FSs, the two directions (i.e., x and y) within the three different structural configurations. An overview of all the simulations within the parametric analysis is listed in Table 4.

Table 4. Summary of the numerical simulations within the parametric analysis.

Design / structural Configuration	Support-Continuity and Orthogonal contribution	Continuity	Section symmetry	Floor equality	Side Face rebars	Failure scenarios	Frame along x-direction	Frame along y-direction
STANDARD	●	○	○	○	○	FS1, FS2, FS3, FS4	✓	✓
CSE+rebars	●	●	●	●	●	FS1, FS2, FS3, FS4	✓	✓
C+rebars	●	●	○	○	●	FS1, FS2, FS3, FS4	✓	✓

With the aim to develop several NLFE simulations, the constitutive laws of the lateral horizontal non-linear springs (Fig. 6) have to be specifically defined. In fact, the structural components orthogonal to each analyzed 2D frame significantly increase the structure's stiffness, imposing restrictions on the lateral displacements [11]-[12],[16]-[18]. The neglect of rotational stiffness is justified by its minimal effect on the flexural peak and its negligible impact on the development of catenary action, as emphasized in [16],[54]. To simulate the contribution provided by the frames orthogonal to the analyzed frame, a translational non-linear spring has been placed at each node of the five floors, as shown, for example, in Fig. 7(b) for the frame FS1-x (i.e., for the first failure scenario in x-direction). The constitutive non-linear laws of the translational springs are properly calibrated through non-linear analyses in SAP2000 [38] conducted on the 3D RC structure. First, the supporting column has been removed to simulate the specific failure scenario and the axial and bending stiffness of beams and columns of the frame under study are nullified since their contributions are accounted for in the 2D NLFE model (e.g., in Fig. 7(b)). The non-linear behavior of the frames within the 3D structure has been modeled using fiber-based plastic hinges placed at specific points in the columns and beams. The length of the plastic hinges has been calculated based on [55]-[56], considering the geometrical characteristics of the cross-sections of the structural elements. In detail, the plastic hinge length is around 50 cm for the beams and 30 cm for the columns. Meanwhile, the number of fibers for each cross-section has been determined through an iterative process to ensure numerical accuracy.

Specifically, the fiber plastic hinges utilized in the model are of "P-M2-M3" type, accounting for both axial force and the two orthogonal bending moments.
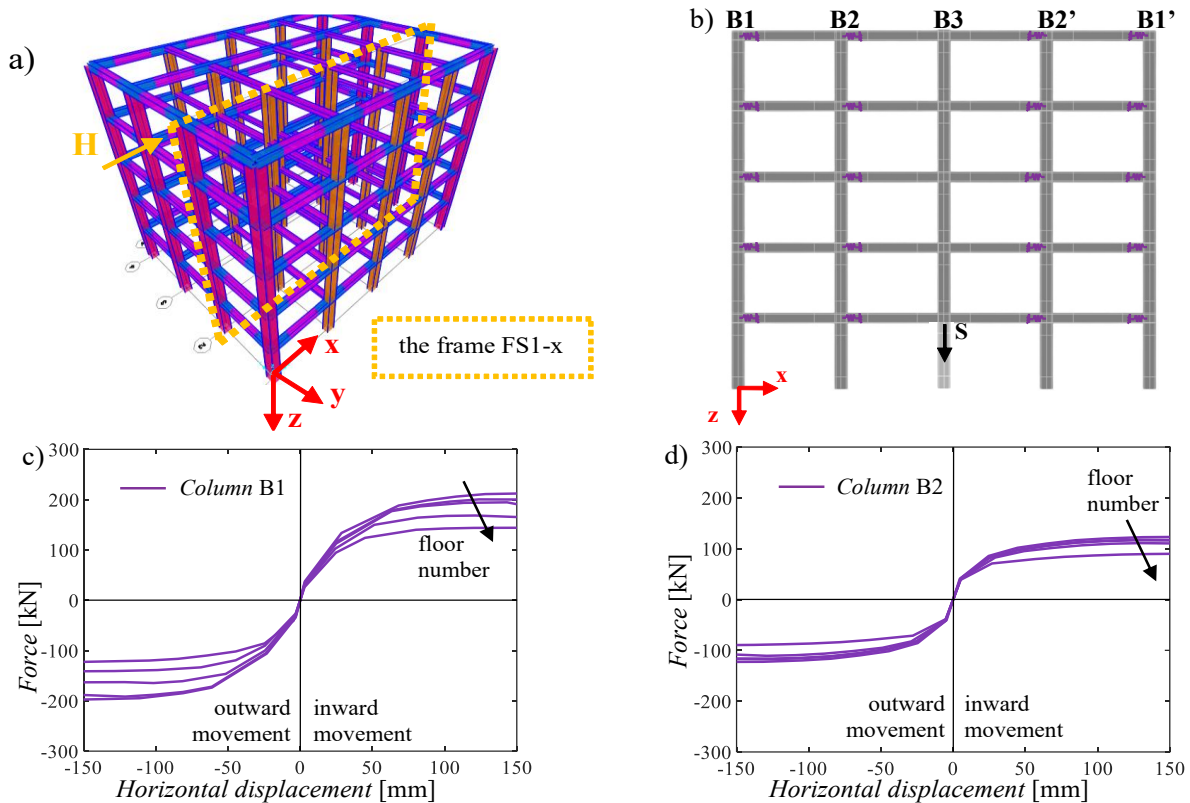

Fig. 7 Lateral constraint conditions: (a) 3D structure modelled in SAP 2000: example of calibration of the constitutive law of a spring for the last floor, column B1, inward direction; (b) springs positions (in purple) within the frame FS1-x in ATENA-2D; (c) constitutive laws of the springs for column B1; (d) constitutive laws of the springs for column B2.
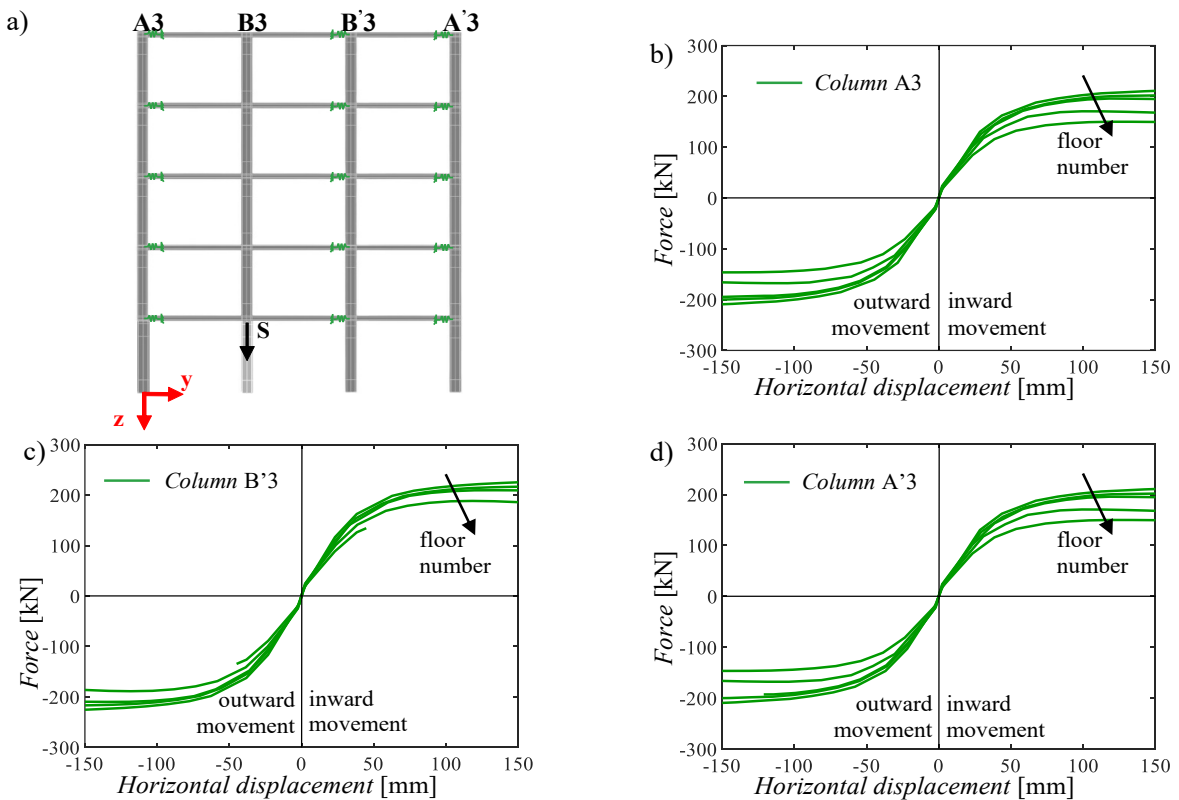

Fig. 8 Lateral constraint conditions: (a) springs (in green) within the frame FS1-y in ATENA-2D; (b) constitutive laws of the springs for column A3; (c) constitutive laws of the springs for column B'3; (d) constitutive laws of the springs for column A'3.

Within the 3D simulations, the geometrical non-linearities are also considered. The contributions provided by slabs having one-way joists (typical characteristics of European constructions) are neglected as marked in [10]. The constitutive laws of both materials, adopted in the 3D model, have been described in Section 4. Then, displacement-controlled numerical analyses have been carried out by imposing, in any node, a horizontal displacement (H) in the out-of-plane direction of the orthogonal frame (e.g., positive x-direction for the example reported in Fig. 7(a)) with step of 1 cm. Furthermore, the constitutive laws have been calibrated for both inward and outward directions, showing differences, slightly more marked at higher stories, between the behaviour in the two opposite directions. Note that the calibration for both directions can be more relevant when the structure is non-symmetric (e.g., presence of staircases or infill walls in a non-symmetric scheme). Each non-linear constitutive law is derived by plotting the force at the analyzed node against the imposed horizontal displacement. This process has been reiterated for each node in all columns except the one experiencing collapse and for each structural configuration and failure scenario. Shear failure was never reached, respecting all the shear verifications. A maximum imposed horizontal displacement of 150 mm was considered since the beam-column nodes do not experience larger displacement during the collapse scenario, as shown in the next sections. As an example, the non-linear constitutive laws are reported in Fig. 7(c)-(d) and Fig. 8(b)-(d) for the "*STANDARD*" configuration and the first failure scenario along, respectively, x- and y- directions. It should be also noted that the springs enter in non-linear field for horizontal displacements larger than around 20 mm.

6. THE FIRST FAILURE SCENARIO: NUMERICAL RESULTS AND COMPARISON

This section describes the removal of column B3, indicated as the first failure scenario FS1. For this failure scenario and the three design configurations, the constitutive laws for the non-linear springs have been calibrated, as previously described in Section 5.

6.1. NLFE analyses along x-direction

This subsection describes the capacity curves of the three configurations for the frame FS1-x, which has deep beams and is subjected to the column removal B3 (i.e., first failure scenario, Fig. 6(a)).

The capacity curve related to the "*STANDARD*" configuration, presented in Fig. 9(a), shows a maximum resistant load in the flexural phase (i.e., $P_{MAX,FL}$) equal to 1129 kN. After that, the capacity curve presents an initial softening phase followed by a starting of catenary effect for a very large displacement (i.e., around 60 cm) visible also from the horizontal displacements of beam-column nodes (Fig. 9(b)) with a very slight increase in the structural resistance. The increase stops when the bars reach their ultimate strain, and this occurs at a maximum ultimate load (i.e., $P_{MAX,ULT}$) equal to 1024 kN, with an imposed vertical displacement of around 64 cm. The vertical displacements of nodes in both columns B1 and B2 (Fig. 9(c)) show a decrease followed by an increase. The initial reduction is a result of the arching behavior of the beams, while the subsequent increase occurs due to the rotation of the nodes in the transition to catenary activation.

The design recommendations in the "*C+rebars*" configuration, specifically, the continuity of the beam's longitudinal reinforcement and inclusion of side face rebars, yield a significant advantage, as demonstrated by the capacity curve together with the horizontal and vertical displacements of the nodes in Fig. 9(a),(d)-(e). The transition towards the catenary phase is considerably anticipated (i.e., at a vertical displacement lower than 20 cm). This enhancement is evident in both the capacity curve and horizontal displacements of the beam-column nodes, where the change in sign is highlighted. This benefit is guaranteed by both design improvements: the reinforcements, having a longer arrangement along the beams, contribute to establish the tying effect at an early vertical displacement; the side face rebars, placed in the central part of the cross-sections, are subjected to low strains during the flexural phase and this helps to anticipate the catenary behavior when tensile forces arise. By observing the horizontal displacements of the beam-column nodes (Fig. 9(b),(d),(f)), the springs enter in non-linear regime when the imposed vertical displacement is larger than 60 cm (i.e., when catenary

effect is already activated) and only along the inward direction, while during the flexural-arching and softening phases the non-linearities are not exploited.
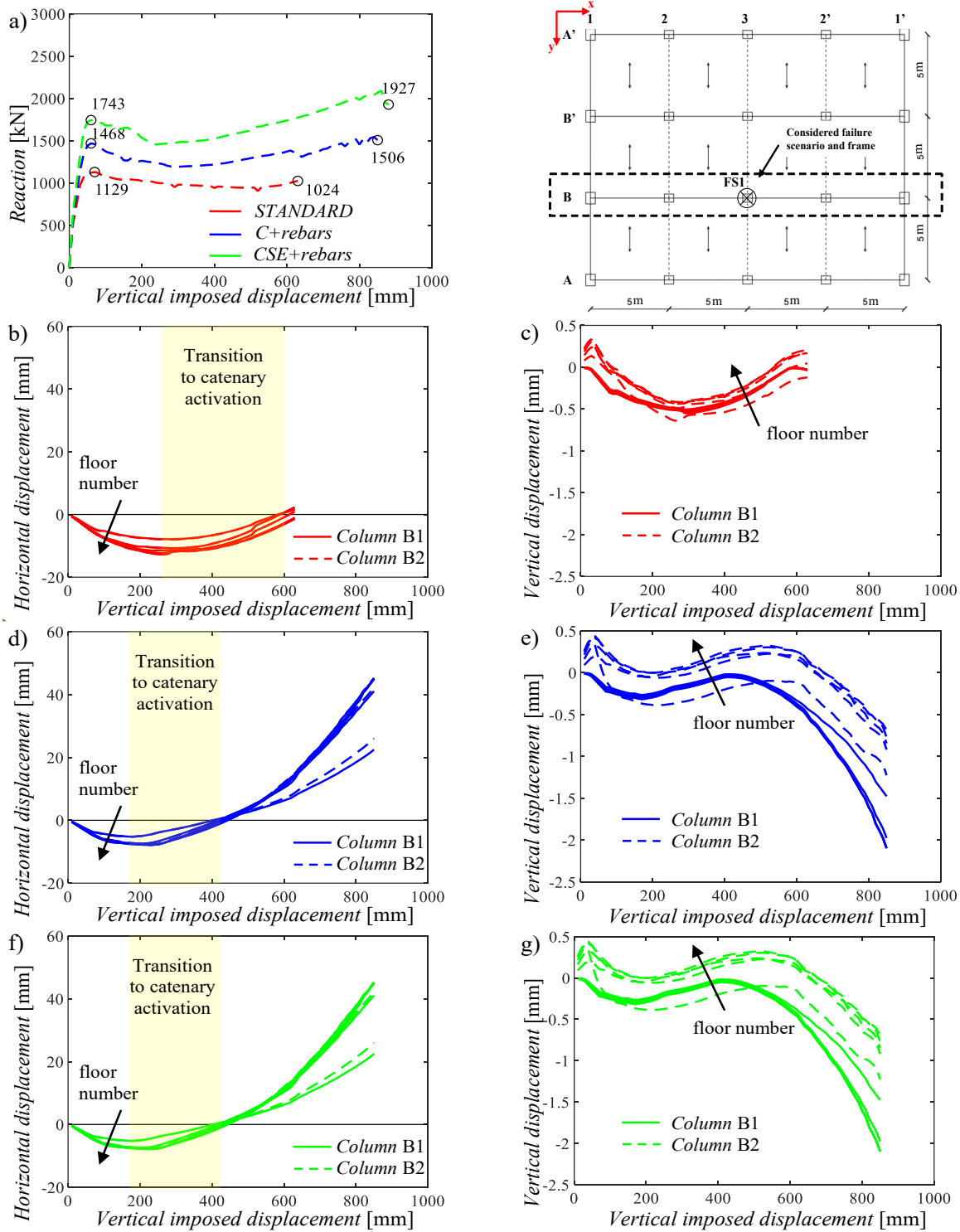

Fig. 9 Results of the displacement-controlled pushdown analyses of the frame FS1-x (i.e., first failure scenario – x-direction): (a) capacity curves; (b),(d),(f) horizontal displacements of the beam-column nodes for *STANDARD*, *C+rebars* and *CSE+rebars* configurations; (c),(e),(g) vertical displacements of the beam-column nodes for *STANDARD*, *C+rebars* and *CSE+rebars* configurations.

Thus, the non-linear calibration for the contribution of the orthogonal frame is crucial, especially, when dynamic phenomena involve large displacements. In addition, there is an increase in both the maximum resistant load during the flexural phase and ultimate resisting load, due to larger quantity of rebars in the beams. The last important advantage is related to ductility because the ultimate strain

for the longitudinal reinforcement (i.e., 18%) is reached at an imposed vertical displacement more than 20 cm later compared to the configuration without the side face rebars. The "*CSE+rebars*" configuration adds equality in the reinforcement arrangements between floors and the symmetry of the cross-sections. This leads to an increase in the amount of reinforcement with the following improvements: both flexural peak and ultimate resistance show higher values and the catenary effect is slightly anticipated compared to the previous configuration (i.e., *C+rebars*), as visible in Fig. 9(a). The longitudinal reinforcement reaches the ultimate strain (i.e., 18%) at an imposed vertical displacement equal to 90 cm.

6.2. NLFE analyses along y-direction

The pushdown analyses have been assessed for frame FS1-y, which is the frame having wide beams and subjected to the removal of column B3 (i.e., first failure scenario) along the y-direction, as described in Fig. 6(b). Fig. 10 reports the capacity curves together with the vertical and horizontal displacements of the beam-column nodes. The results in terms of capacity curves exhibit a behavior that is entirely different from the capacity curve illustrated in Subsection 6.1. In this case, regarding the three design solutions, the flexural phase concludes with a maximum resistant load equal to 159 kN, which is significantly lower (Fig. 10(a)). This difference depends on the lower amount of reinforcement in the wide beam (i.e., 2 ϕ14 in the upper chord and 2 ϕ14 in the lower chord of the cross-section). The curves demonstrate a transition of catenary activation occurring between 15 and 20 cm of the imposed vertical displacement, thereby considerably anticipating the catenary phase. The catenary phase is not only anticipated but significantly more pronounced with a maximum resistant load much bigger than the one recorded at the flexural peak. This can be attributed to the following reasons: i) the longitudinal reinforcement of the wide beams is continuous along the length of the structural elements starting from the *STANDARD* configuration and this helps to develop the tying effect; ii) the wide beams are significantly more ductile than the deep beams [37]. By observing the horizontal displacements of the beam-column nodes (Fig. 10(b),(d),(f)), the springs enter in non-linear regime when the imposed vertical displacement is larger than 35 cm (i.e., when catenary effect is already mobilized). Thus, the non-linear field for the translational springs is reached earlier for the frames in y-direction if compared to the frame in x-direction. For this reason, the non-linear calibration of the springs laws is very important. Again, the non-linearities are not involved during the outward movement of the beam-column nodes (i.e., flexural-arching phase and softening phase) but only for inward movements (i.e., catenary phase).

From these capacity curves, it can also be observed that there is only a small difference between *STANDARD*, *C+rebars* and *CSE+rebars* configurations since the wide beams are not subjected to the different design modifications. The minimal differences in the results are attributable to the non-linear translational springs, which were recalibrated considering the design improvements on the other structural elements (i.e., longitudinal and transverse reinforcement of beams and stirrups of the joints) of the 3D building in both *C+rebars* and *CSE+rebars* configurations. In fact, those differences can be noticed at very large vertical displacements.
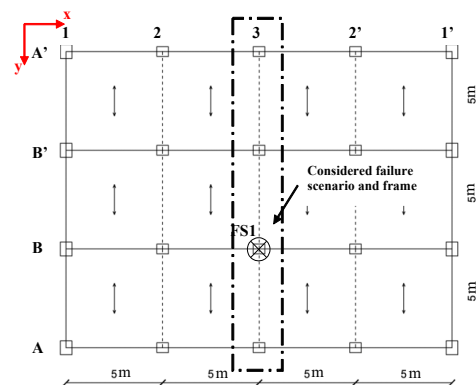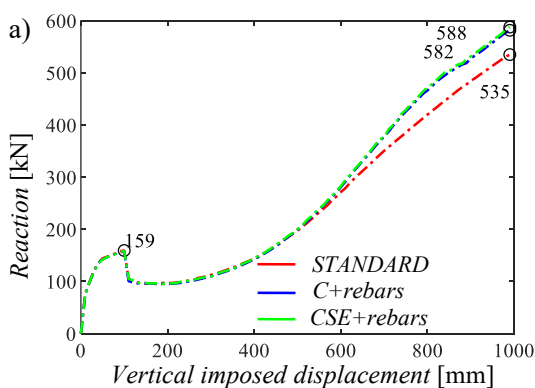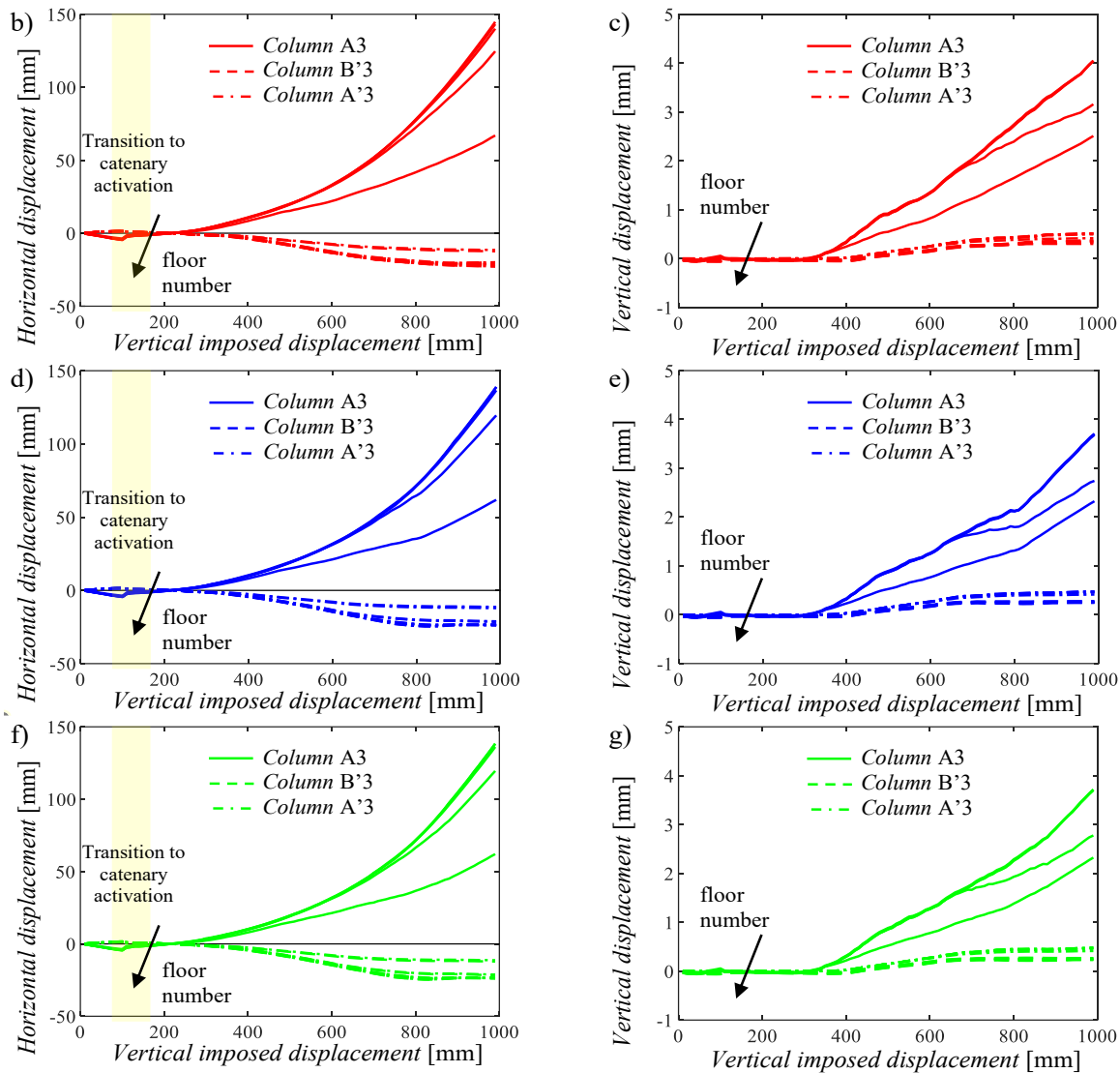
Fig. 10 Results of the displacement-controlled pushdown analyses of the frame FS1-y (i.e., first failure scenario – y-direction) (a) capacity curves; (b),(d),(f) horizontal displacements of the beam-column nodes for *STANDARD*, *C+rebars* and *CSE+rebars* configurations; (c),(e),(g) vertical displacements of the beam-column nodes for *STANDARD*, *C+rebars* and *CSE+rebars* configurations.

6.3. *Superposition of the capacity curves*

The proposed idea of Section 2 is to superimpose the 2D NLFE capacity curves to obtain the corresponding global capacity curve representing the behavior that the 3D frames exhibit for the loss of a column. To achieve this, the capacity curves obtained for the two frames, mutually orthogonal, subjected to the loss of the same column in the first collapse scenario FS1 (i.e., column B3) were superimposed, as also experimentally performed for a substructure in [54]. This procedure has been repeated for the three different configurations to compare the advantages of the design suggestions. From Fig. 11, it can be deduced how the frame FS1-y (i.e., the frame with wide beams), presenting a much lower flexural peak than the frame FS1-x, offers a minimal contribution in the flexural phase until the maximum resistant load. This contribution gradually increases for larger imposed displacements due to the greater ductility of the frames with the wide beams, as described in Subsection 6.2. This behavior is shown in the superimposed capacity curves for all the three configurations. In addition, for all the structural configurations, the frame along y-direction leads to the transition towards catenary activation for smaller imposed vertical displacements with ultimate resistances (governed by the failure of the FS1-x frame) greater than the flexural peaks (i.e., Fig. 11). This last improvement is particularly evident in the *C+rebars* and *CSE+rebars* configurations (i.e., 1990 kN and 2200 kN, respectively, which are higher than the flexural peaks equal to 1600 kN and

1900 kN, respectively). This ensures a higher level of safety in the case of events involving the loss of a column for these two configurations. The global capacity curve, for the *STANDARD* configuration (Fig. 11(a)), shows a vertical drop followed by an increasing of the resistance at around 60 cm. This trend is due to the overcome of the ultimate strain in the beam longitudinal reinforcement (i.e., 18%) in the frame along the x-direction (i.e., seismic-resistant frame). After that, the only contribution comes from the orthogonal frame in the y-direction. This trend is the same for both *C+rebars* (Fig. 11(b)) and *CSE+rebars* (Fig. 11(c)) models, but with a larger ultimate vertical displacement (i.e., 87 cm and 89 cm, respectively).
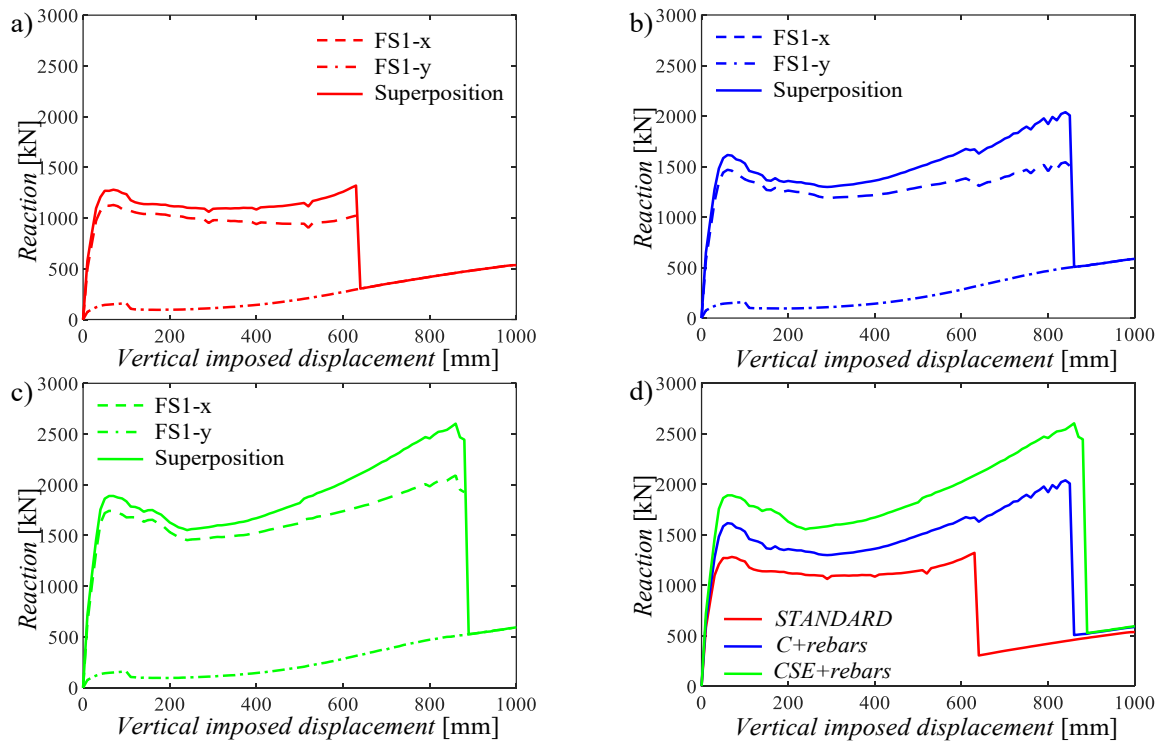

Fig. 11 Results of the superposition of the capacity curves for the first failure scenario FS1: (a) global capacity curve for the *STANDARD* configuration; (b) global capacity curve for the *C+rebars* configuration; (c) global capacity curve for the *CSE+rebars* configuration; (d) comparison between the global capacity curves for the three configurations.

From the comparison, it follows that, for the first failure scenario, the model with continuity of the beam longitudinal reinforcement and presence of the side face rebars (i.e., *C+rebars* configuration) represents the best balance between improving the robustness of the structure and sustainability principles since lower amounts of longitudinal reinforcement are arranged.

6.4. Comparison with the 3D model

To assess the effectiveness of the global capacity curves obtained through the superposition of the 2D NLFE analyses on the two orthogonal frames affected by the first failure scenario, a 3D displacement-controlled pushdown non-linear analysis has been performed on the 3D model in SAP2000 [38], defined in Section 5. The constitutive laws of both materials, adopted in the 3D model, are described in Section 4. The analysis consists in applying an increasing vertical displacement, with step of 1 cm, at the top of the removed supporting column (i.e., column B3), and determining the force exerted by the remaining structure at that specific point. Within the 3D simulations, the geometrical non-linearities are also considered. Note that non-linearities are concentrated in both beams and columns of the frames through fiber plastic hinges, as explained in Section 5.

In Fig. 12, the 3D capacity curve obtained from the 3D model is compared with the global capacity curve obtained from the superposition of the 2D NLFE analyses. The main difference is in softening stage with a lower resistance reduction in the 3D model. This aspect derives from modeling discrepancies between the software codes used. In the case of the non-linear static analysis conducted

on the 3D model, the non-linearities of the structure are concentrated in the fiber-based plastic hinges, which consider only the interaction between axial force and bending moment, neglecting interaction with shear force together with a different modelling of the evolution of concrete cracking. In addition, the presence of the stirrups is not modelled in the 3D model but only the confinement effects are included, whereas in the NLFE analyses, the stirrups are modelled as discrete truss elements. However, it can be noticed that the flexural peak, for example, in the 3D *STANDARD* model is equal to 1280 kN that is very similar to the value obtained in the global capacity curve (i.e., 1284kN). The extension of the softening phase and catenary phase are also quite identical. The final drop in resistance also occurs for both models at the same vertical displacement value. It follows that the global capacity curve evaluated with the superposition principle underestimates the reaction with respect to the 3D model, implying results on the safe of safety. To conclude, the results confirm the effectiveness of the superposition of the 2D capacity curves, achieved with a reduced computational effort. The differences fall within the epistemic uncertainty topic [57]-[60]. The superposition in non-linear field fails only for the column subjected to the loss but the other structural elements work together respecting the deformability compatibility, as also demonstrated in [19].
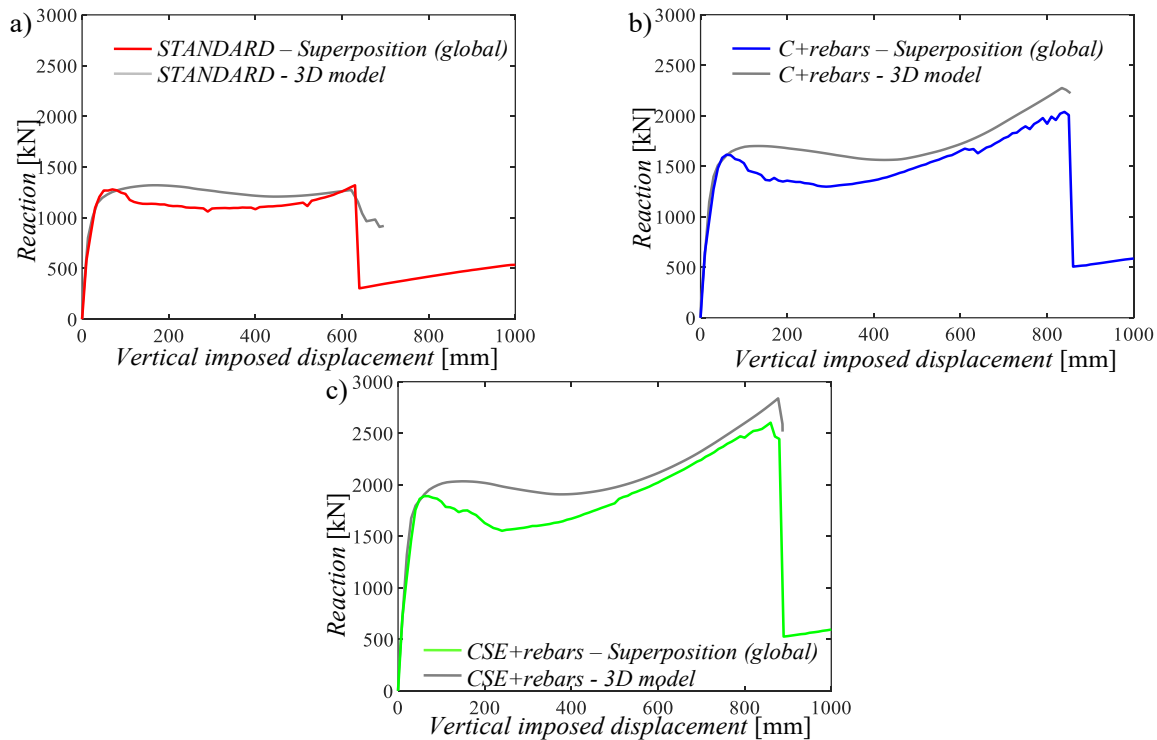

Fig. 12 Comparison between global capacity curves and 3D capacity curves for the first failure scenario FS1.

7. THE SECOND FAILURE SCENARIO: NUMERICAL RESULTS AND COMPARISON

This section describes the removal of column B2, indicated as the second failure scenario FS2. For this failure scenario and the three structural configurations, the constitutive laws for the non-linear springs have been re-calibrated following the method described in Section 5.

7.1. NLFE analyses: superposition of the capacity curves along x- and y- directions

The capacity curves of the frame FS2-x and FS2-y are shown in Fig. 13 for all the three design configurations. More detailed results in terms of both horizontal and vertical displacements of the beam-column nodes are given in Appendix B (Fig. B1 and Fig. B2).

As for the frame with deep beams along x-direction, the *STANDARD* configuration (Fig. 13(a)) exhibits a lower flexural peak and ultimate resistance compared to the first collapse scenario as well as the catenary effect is absent. This is because of the reduced contribution from the orthogonal frames in the second failure scenario. It is possible to understand how the presence of the side face rebars in

the *C+rebars* configuration (Fig. 13(b)), similarly to the first failure scenario, leads to an increase in the flexural peak and facilitate the activation of the catenary effect (at a displacement of around 20 cm). Similar conclusions can be drawn regarding the *CSE+rebars* configuration (Fig. 13(c)).
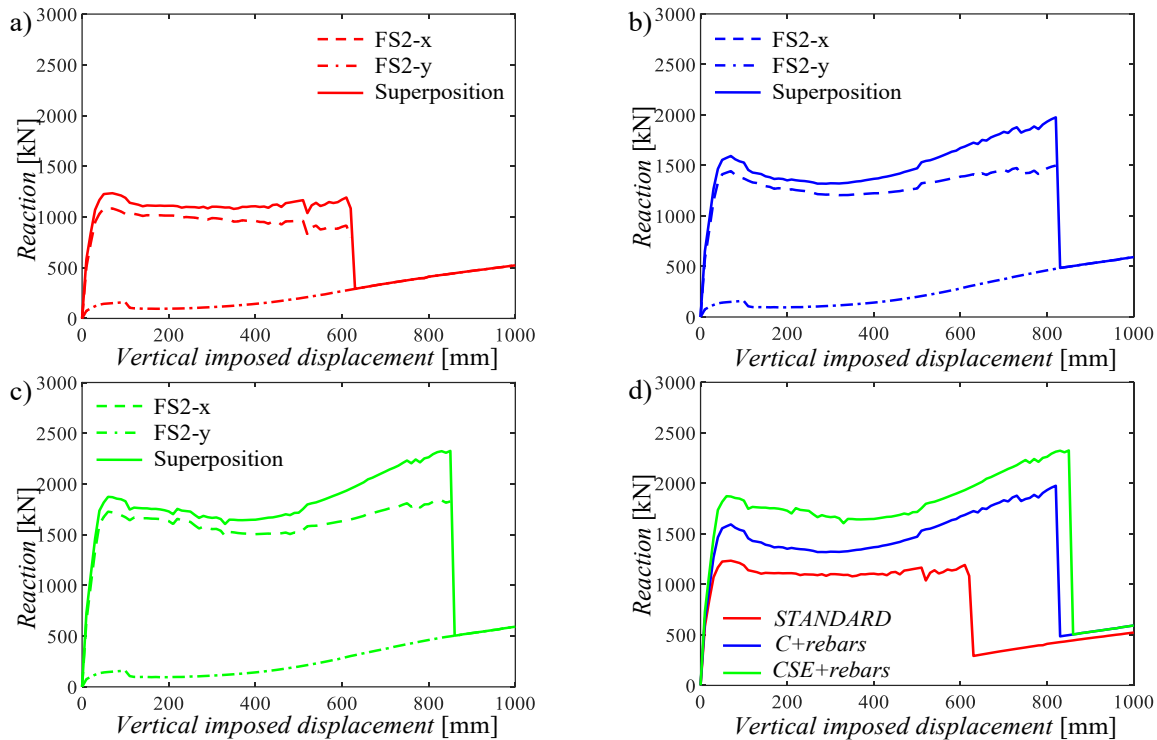

Fig. 13 Results of the superposition of the capacity curves for the second failure scenario FS2: (a) global capacity curve for the *STANDARD* configuration; (b) global capacity curve for the *C+rebars* configuration; (c) global capacity curve for the *CSE+rebars* configuration; (d) comparison between the global capacity curves for the three configurations.

The capacity curves, obtained for the frame with wide beams along y-direction (i.e., FS2-y), are similar to those reported in Subsection 6.2: the flexural phase is significantly lower compared to the value reached for the orthogonal collapsed frame, but the transition of catenary is considerably anticipated and more pronounced. Comparing the global capacity curves (Fig. 13(d)), the *CSE+rebars* configuration exhibits increased flexural and ultimate resistance in comparison to the *C+rebars* configuration also with a higher vertical imposed displacement at collapse.

Even in this failure scenario, the *C+rebars* configuration represents the optimal balance between enhancing structural robustness and promoting sustainability. Furthermore, as also visible in Appendix B (Fig. B1 and Fig. B2), the calibration of the non-linear translation springs can be crucial for this failure scenario to capture the response also during the initial flexural-arching phase for the frame in x-direction (Fig. B1) but especially at large displacements (i.e., catenary phase) for both frames (Fig. B1 and Fig. B2). In fact, the beam-column nodes of the frame F2-x and, especially, frame F2-y are subjected to horizontal displacement larger than 20 mm (i.e., value at which the non-linearities of the translational springs are activated) both for inward and outward movements.

7.2. Comparison with the 3D model

Also for the removal of column B2 (i.e., the second failure scenario), displacement-controlled pushdown analyses have been performed on the 3D structure in SAP2000 [38], as shown in Fig. 14. Comparable findings can be derived for the second failure scenario: the flexural peaks in the 3D models closely mirror the values of the global capacity curves even if at vertical displacements slightly higher in the 3D model; the transition through catenary effect is quite coincident as well as the final drops in resistance happen at identical vertical displacements and the results of the superimposed approach are on the safe side if compared to the 3D model. Being the second FS more demanding in terms of local stresses, higher differences between the global and 3D curves are in the

softening phase due to cracking and crushing of concrete. These results however confirm the effectiveness of the superposition of the 2D capacity curves also for the second FS.
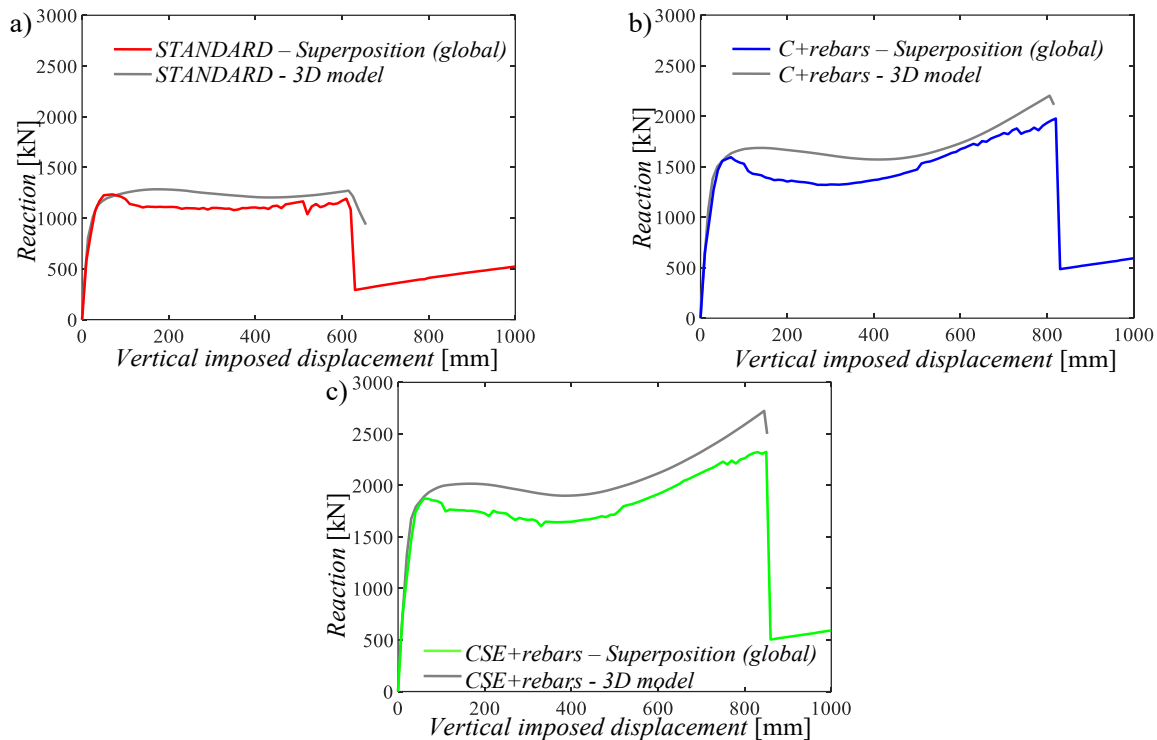

Fig. 14 Comparison between global capacity curves and 3D capacity curves for the second failure scenario FS2.

8. THE THIRD FAILURE SCENARIO: NUMERICAL RESULTS AND COMPARISON

This section deals with the third failure scenario FS3 (i.e., removal of column A2) for the *STANDARD*, *C+rebars* and *CSE+rebars* configurations. The constitutive laws governing the non-linear springs have been re-calibrated using the approach outlined in Section 5.

8.1. NLFE analyses: superposition of the capacity curves along x- and y- directions

The global capacity curves for the frame FS3-x and FS3-y are reported in Fig. 15 for the three structural configurations. More detailed results in terms of both horizontal and vertical displacements of the beam-column nodes are given in Appendix B (Fig. B3 and Fig. B4). These results underline that the calibration of non-linear springs can be relevant for this failure scenario when the removed column is not a perimetral one (i.e., for the frame in x-direction) and for both outward and, especially, inward movements of the beam-column nodes. Differently, for the frame in y-direction the horizontal displacements of the beam-column nodes are very low (i.e., much lower than 20 mm) and the springs remain in linear regime. The frame in the x-direction having deep beams and subjected to collapse is, unlike what was observed in the first two collapse scenarios, a perimeter frame (i.e., frame FS3-x), and the beams have a slightly lower quantity of longitudinal reinforcement compared to the ones of the frames FS1-x and FS2-x, as reported in Table 1. The capacity curves reported in Fig. 15 show, in the *STANDARD* configuration, the lowest flexural peak among the three cases analyzed, and an absence of catenary effect. The increased presence of the bars generates an increase in the flexural peak, as observed in the *C+rebars* and *CSE+rebars* configurations. The transition towards the catenary effect is present in both the *C+rebars* and *CSE+rebars* configurations. On the frame FS3-y having wide beams, only a slight catenary effect is observed, starting around 20 cm of imposed vertical displacement. The contribution of the frame FS3-y is very reduced with respect to the first and second collapse scenarios. It should be noted that, for the frame FS3-y, the confinement effects in the beams in terms of constitutive laws of concrete in compression are not included since the failure involves a perimeter column (i.e., column A2). Therefore, the resisting mechanism primarily relies

on the orthogonal beams. Even in this case, the *C+rebars* configuration represents a good trade-off between enhancing structural robustness and promoting sustainability.
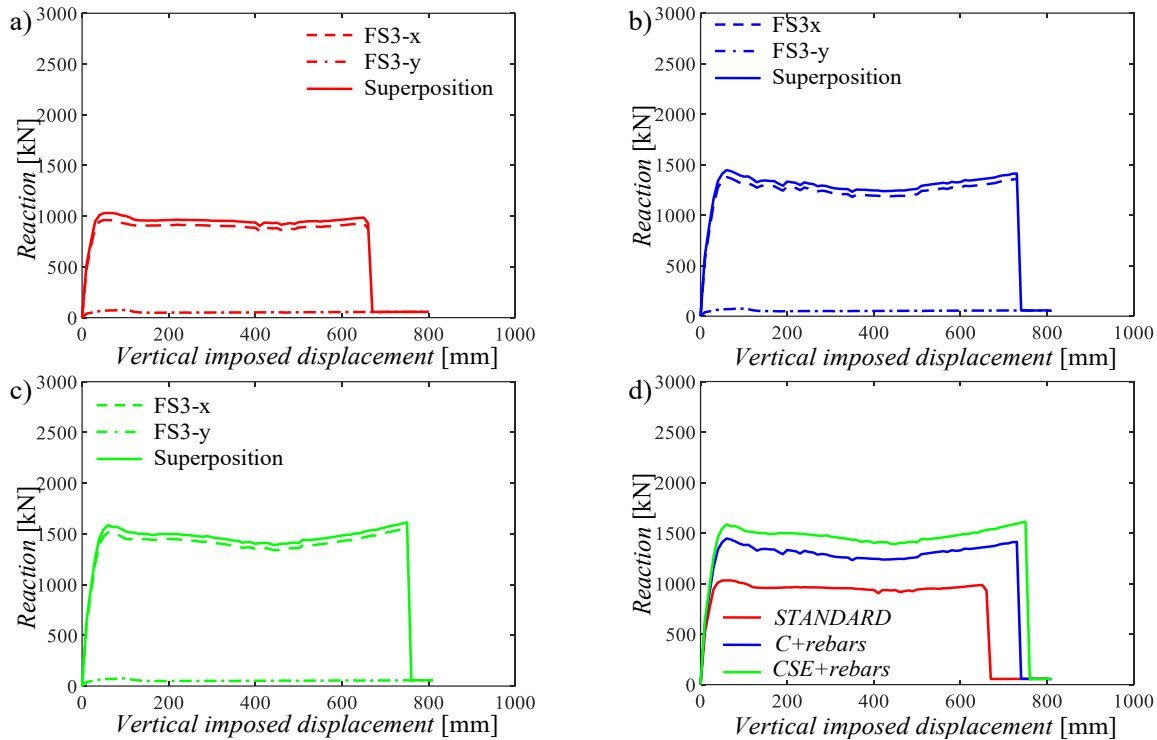

Fig. 15 Results of the superposition of the capacity curves for the third failure scenario FS3: (a) global capacity curve for the *STANDARD* configuration; (b) global capacity curve for the *C+rebars* configuration; (c) global capacity curve for the *CSE+rebars* configuration; (d) comparison between the global capacity curves for the three configurations.

8.2. Comparison with the 3D model

Fig. 16 depicts the comparison between the global capacity curves derived in the previous subsection and the 3D capacity curves obtained on the 3D structure in SAP2000 [38].
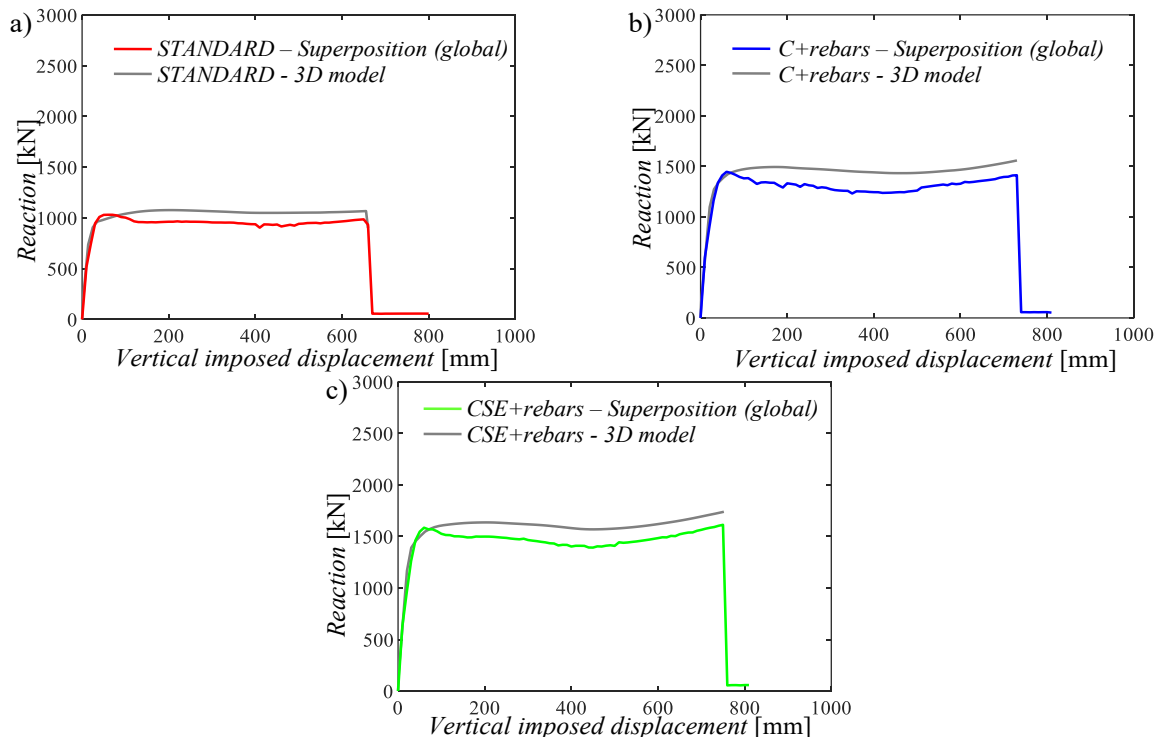

Fig. 16 Comparison between global capacity curves and 3D capacity curves for the third failure scenario FS3.

Also for the third failure scenario, 3D displacement-controlled pushdown non-linear analyses have been carried out after the removal of column A2, neglecting properly the confinement effects in the beams as done for the global capacity curve. The flexural peaks are similar, although, occur at slightly higher vertical displacements in the 3D curves. The catenary effects are similar and the reductions in resistance occur at the same vertical displacement. Again, the results of the proposed superposition are confirmed and are on the safe side.

9.   THE FOURTH FAILURE SCENARIO: NUMERICAL RESULTS AND COMPARISON

This section describes the fourth collapse scenario FS4, involving the removal of column A1, for the *STANDARD*, *C+rebars* and *CSE+rebars* configurations. The non-linear laws of the springs have been recalibrated following the methodology detailed in Section 5.

9.1. NLFE analyses: superposition of the capacity curves along x- and y- directions

The capacity curves related to the x- and y- directions and superpositions are reported in Fig. 17. More detailed results in terms of both horizontal and vertical displacements of the beam-column nodes are given in Appendix B (Fig. B5 and Fig. B6).
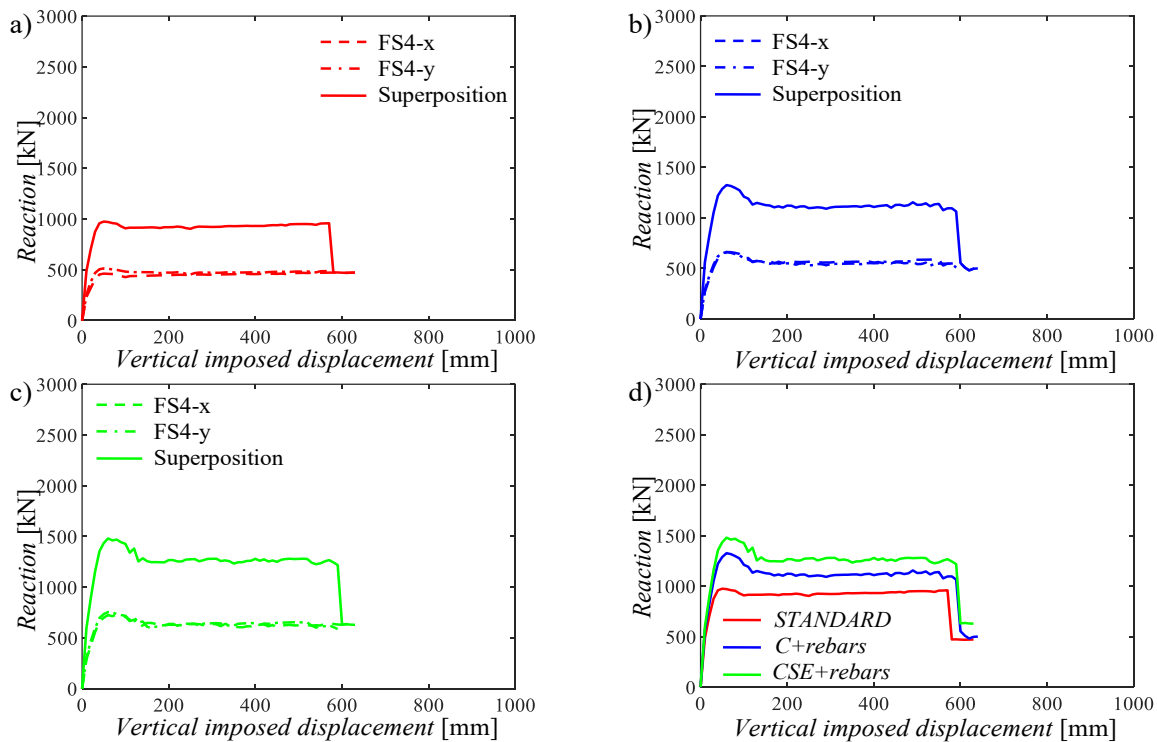

Fig. 17 Results of the superposition of the capacity curves for the fourth failure scenario FS4: (a) global capacity curve for the *STANDARD* configuration; (b) global capacity curve for the *C+rebars* configuration; (c) global capacity curve for the *CSE+rebars* configuration; (d) comparison between the global capacity curves for the three configurations.

In these figures of Appendix B, it is demonstrated how the calibration of non-linear springs is not so relevant for this failure scenario since the horizontal displacements of the beam-column nodes in both frames are much lower than 20 mm and the springs remain in linear regime. This is due to the fact that the removed column is a perimetral one for both frames along x- and y-directions.

The frame FS4-x is perimetral and features deep beams with a slightly lower quantity of longitudinal reinforcement compared to the ones of the frames FS1-x and FS2-x and equal to the frame FS3-x. However, the removed column is a side one as shown in Fig. 6(g). The capacity curves reveal that the *STANDARD* configuration exhibits the smallest flexural peak, lack of the catenary effect and the resistance presents a plateau until the ultimate strain for the longitudinal reinforcement (i.e., 18%) at around 60 cm of imposed vertical displacement. Notably, the capacity curves, associated to the enhanced configurations, are characterized by larger flexural peak with respect to the *STANDARD*

case. This implies higher internal energy and, thus, capability to find the performance point (as described in Section 2) for lower imposed vertical displacement. The capacity curves in y-direction are different from the ones for the first three collapse scenarios because the beams of FS4-y have dimensions of 40x50 cm (i.e., they are deep beams). Thus, the capacity curves in x- and y- directions for this failure scenario are very similar. It should be noted that both the frames FS4-x and FS4-y are subjected to a failure scenario involving the perimetral column and, thus, the confinement effects in the beams in terms of constitutive laws of concrete in compression are not modelled. Again, the *C+rebars* configuration represents a good balance between enhancing structural robustness and promoting sustainability.

9.2. Comparison with the 3D model

Fig. 18 illustrates a comparison between the global capacity curves derived in the previous subsection and the capacity curves obtained from displacement-controlled pushdown non-linear analyses on the 3D structure in SAP2000 [38], neglecting properly the confinement effects.
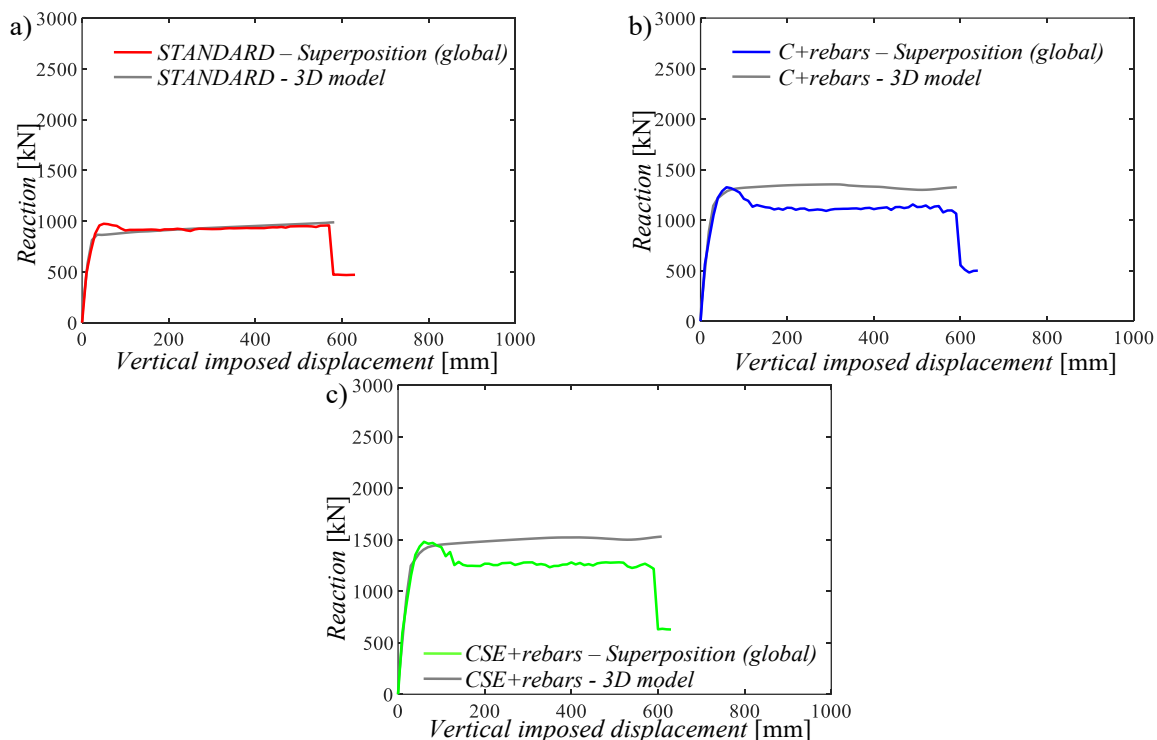

Fig. 18 Comparison between global capacity curves and 3D capacity curves for the fourth failure scenario FS4.

Even if the ultimate resistance is reached for a similar value of imposed vertical displacement, there are some differences in the ultimate resistance. This is due to the cracking in concrete as well as to the model uncertainties in both numerical approaches. These results, however, confirm a good agreement between global and 3D capacity curves also for the fourth FS even if the former leads to safer results apart from the prediction of the flexural peak achieved in the *STANDARD* model.

10. ENERGETIC APPROCH FOR THE FOUR FAILURE SCENARIOS

According to the energetic approach by Izzuddin [27] discussed in Section 2, the performance point due to an accidental column removal is reached where the external work W_{ext}, i.e., the work done by the gravity loads, is equal to the internal energy U_i, i.e., the energy absorbed by the structure. The former is computed as the product between the gravity loads concentrated in the point of the column removal and vertical displacement in the same point. The internal energy U_i is equal to the area under the global capacity curve.
Fig. 19 shows the comparison between internal energy and external work in terms of performance points for the three different design configurations and four different failure scenarios. As can be

observed, for the first (Fig. 19(a)) and second (Fig. 19(b)) failure scenarios, the performance is never reached for the *STANDARD* configuration, while is reached for vertical displacements between 5 and 10 cm for the other two structural configurations. In addition, it is important to note that for the third (Fig. 19(c)) and fourth (Fig. 19(d)) failure scenarios, even if the presence of infill walls is omitted in the structural model but it considered as external loads, the energy balance is always obtained. In fact, in these cases, the external work is lower due to the lower magnitude of the effective area with respect to the first two scenarios. This is in line with the considerations in [61], in fact failures originating in internal areas generally impose greater horizontal loads on the remaining structure than those in edge or corner zones, as they affect a larger collapse influence area.
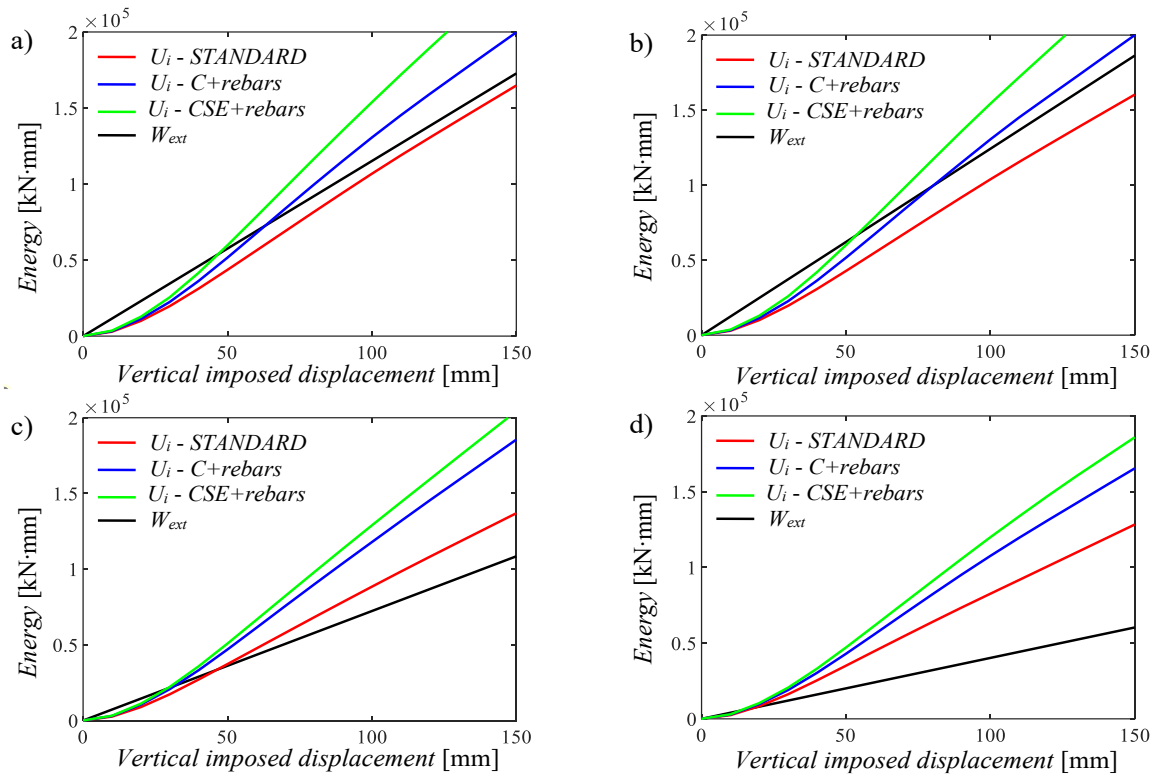

Fig. 19 Energy-balance approach to compare the three design configurations with respect to the: (a) first failure scenario-FS1; (b) second failure scenario-FS2; (c) third failure scenario-FS3; (d) fourth failure scenario-FS4.

It should be underlined that the calibration of non-linear springs is essential to determine the behavior of the 3D structure, when the goal is to capture the non-linear effects (i.e., softening and catenary stage) and can be important also for the performance point for some design configurations and failure scenarios (e.g., FS3) although the very low vertical displacements in all failure scenarios.

This energetic analysis leads to define the *C+rebars* configuration as the optimal balance between enhancing structural robustness and promoting sustainability, that represents a key aspect in the occurrence of extreme events.

11. CONCLUSIONS

This work describes the robustness assessment of ordinary 3D RC MR structures by studying the response of the orthogonal plane frames involved in the same failure scenario. The buildings, having slabs with one-way joists, are in a highly seismic zone and characterized by both non-seismic-resistant frames with wide beams and seismic-resistant ones with deep beams. In detail, the three buildings correspond to three different structural configurations: the configuration designed according to the actual code rules and other two configurations where the layout of the longitudinal reinforcement of the beams is modified according to robustness recommendations (i.e., including symmetric amount of reinforcement between the lower and upper chord, continuity, Vierendeel criteria and side face rebars). For each of the three design configurations, four different failure scenarios are studied,

involving the removal of both central and lateral supporting columns. For each failure scenario and structural configuration, 2D NLFE simulations are carried out by studying the response of the frames in the two orthogonal directions with respect to the failed column. In any 2D NLFE simulation, the contribution of the frames, located along the orthogonal out-of-plane direction, is considered by means of translation springs having non-linear constitute laws and placed in each beam-column node of the plane frame under investigation. The force-displacement relationships of these springs are calibrated through 3D fiber-based non-linear analyses by removing the supporting column, applying increasing translational displacements along both outward and inward directions in each beam-column node, showing some differences between the two directions at higher stories. After the spring calibration, an increasing displacement at the top of the removed columns is imposed in the 2D NLFE models to define the corresponding plane capacity curves (i.e., displacement-reaction curves). Successively, the two plane NLFE capacity curves are superimposed to define the global capacity curve of each structure for any failure scenario.

The following conclusions can be drawn:

- the results have demonstrated the importance to calibrate the non-linear constitutive laws for the springs, especially, for some failure scenarios as well as for large vertical displacements (i.e., after the softening stage) when the removed column is not a perimetral one. This is essential to capture the catenary response, especially, for wide beams that provide an important contribution in terms of ductility. In addition, the different calibration between the two in-plan directions can be very relevant for asymmetrical systems (e.g., when the presence of staircases or infill walls is accounted for);
- the response superpositions are validated through the comparison with the 3D capacity curves derived from 3D fiber-based non-linear analyses. The importance of this validation is the possibility to study the response of 3D frames, having frames with different geometries and resisting characteristics, under a supporting column removal scenario without the need to perform computationally heavy 3D analyses;
- the adopted robustness improvements have demonstrated beneficial effects in increasing the bearing capacity of the system and/or anticipating the catenary behaviour in any failure scenario. This is important, especially, for the frames having deep beams, where the side face rebars are essential to favour the catenary mechanism. These improvements have also demonstrated to be effective in increasing the ductility of the system;
- the energetic equivalence approach has been applied on the global capacity curves to compute the performance point for each of the three design configurations and four failure scenarios. The outcomes have highlighted how also for the most demanding failure scenarios, the inclusion of robustness criteria (e.g., side face rebars) in the design of the plane MR frames allows to reach a performance point for low vertical displacement enhancing the structural robustness. This is not the case of the building designed according to actual code rules, where the performance point was not reached.

Therefore, the design of 3D RC structures can be performed by means of the design of the MR frames accounting for some relevant 3D effects by means of non-linear translational springs and superimposing the effects of the planar NLFE responses on the two orthogonal directions as well as respecting both seismic and robustness principles. The robustness improvements of the *C+rebars* configuration (i.e., with criteria of continuity and side face rebars) represent an optimal balance between enhancing structural robustness and promoting sustainability in the occurrence of extreme events.

In the end, it should be underlined that the study does not account for any staircase and the membrane effects of the slab are discarded since they are less relevant in case of one-way joists slabs, as the typology of the building investigated in the study.

ACKNOWLEGEMENTS

APPENDIX A

This appendix defines the numerical model calibrated to reproduce the results of an experimental test [31] on a beam-column subassembly extracted from a 10-story building designed in Seismic Category D according to ACI 318 Building Code [62]. The experimental test is selected since it has similar characteristics with respect to the case study of the present work. In detail, the sub-assembly (Fig. A1) is composed by two beams having a length of 5.5m and two columns of around 4.5m height. The beams have a cross-section of 71.12x50.8cm^2 and are reinforced with 2 bars of 28.65mm diameter in the lower chord and 4 or 2 bars of 25.4mm diameter in the upper one for, respectively, dissipative and non-dissipative area. The dissipative area has a length of 1.83m. The transverse reinforcement is composed of 2-leg stirrups having 12.7mm diameter with a step of 22.8cm or 10.16cm, respectively, in non-dissipative and dissipative areas. As for the columns, their cross-section is squared and has a size of 71.12cm, while their longitudinal reinforcement is made of 12 bars of 25.4mm diameter and the 4-leg stirrups have a step of 10.16mm and a diameter of 12.7mm.

Regarding the loading scheme, a displacement-controlled application of the load is assumed, by means of 4 hydraulic rams placed on top of the central column and imposing a rate of 25mm/minute. Four steel rods are fixed to the reaction wall to prevent any out-of-plane movement. Two concrete blocks are placed on the internal side of the upper part of the lateral columns and fixed to the reaction wall. Those concrete blocks are then connected to the column by means of 51mm steel plates constrained by four 32mm post-tensioning bars anchored to the columns themselves. The clamping force is 2669kN. Those constraint conditions are representative of a roller-fixture (i.e., prevention of horizontal displacement). Finally, the longitudinal bars of the columns are fully embedded by two footings having width, thickness and height of 2.235x1.626x1.067m^3, respectively.

As for the material properties, a campaign led to the following mean values of the mechanical properties:
-    concrete compressive of 32MPa;
-    concrete tensile strength of 3.1MPa;
-    top bars of the beams (with diameter of 25.4mm): f_y(steel yield strength)=476MPa, f_u(steel ultimate strength)=648MPa, ε_s(ultimate strain)=0.21;
-    bottom bars of the beams (with diameter of 28.65mm): f_y=462MPa, f_u=641MPa, ε_s=0.18;
-    bars of the columns (with diameter of 28.65mm): f_y=483MPa, f_u=690MPa, ε_s=0.17;
-    stirrups (with diameter of 10.16mm): f_y=524MPa, f_u=710MPa, ε_s=0.14.
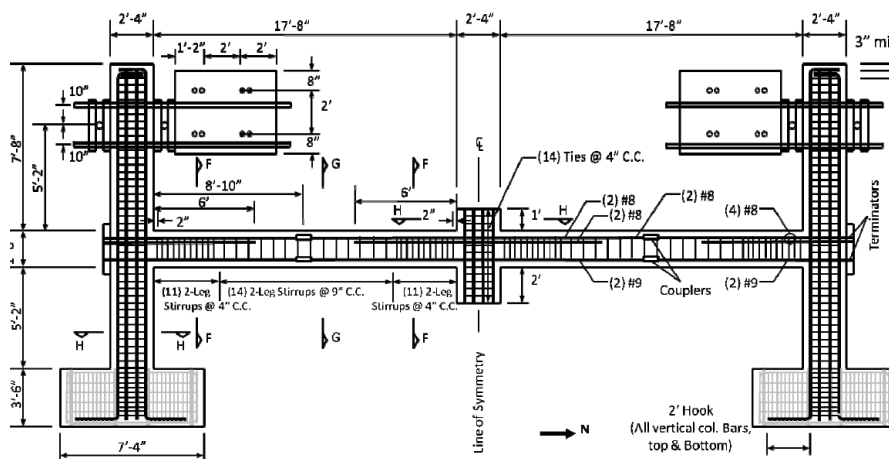

Fig. A1 Geometrical characteristics and cross-sections of the experimental test in [31] (modified from [31]).

The experimental test is reproduced in Atena 2D [39], by taking advantage of the symmetry of the problem (Fig. A2): in fact, no horizontal movements are registered in correspondence of the center line during the test. Distinction is made between concrete core and concrete cover by considering macro-elements made of plane stress quadrilateral isoparametric finite elements, based on linear

polynomial interpolation, with 4 Gauss integration points. The thickness of the macro-elements is set equal to 0.7112m for all the structural elements (i.e., beam, columns and beam-column nodes), in line with the geometrical out-of-plane dimension. The mesh size varies in the range between 0.05m and 0.10m, in line with a sensitivity analysis finalized to capture the experimental response. The bars are considered as discrete elements.
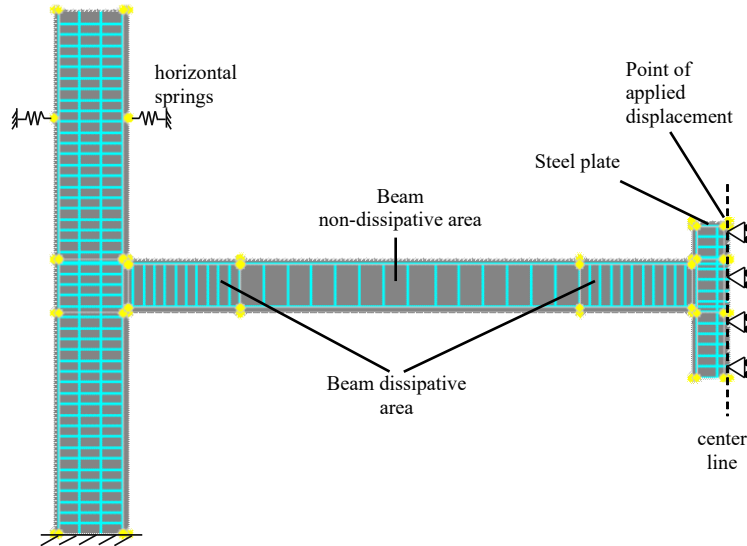

Fig. A2 Representation of the FE modeling of half of the sub-assembly: joints, macro-elements and discrete bars.

The constraint conditions are the following (Fig. A2): horizontal movements in correspondence of the center line are avoided in order to respect the symmetry of the problem; fixed horizontal and vertical movement at the base of the columns in correspondence of half of the height of the footing; two springs (with a properly calibrated stiffness of almost 140N/mm) are placed at around 30cm from the top of the column to represent the roller-fixture.
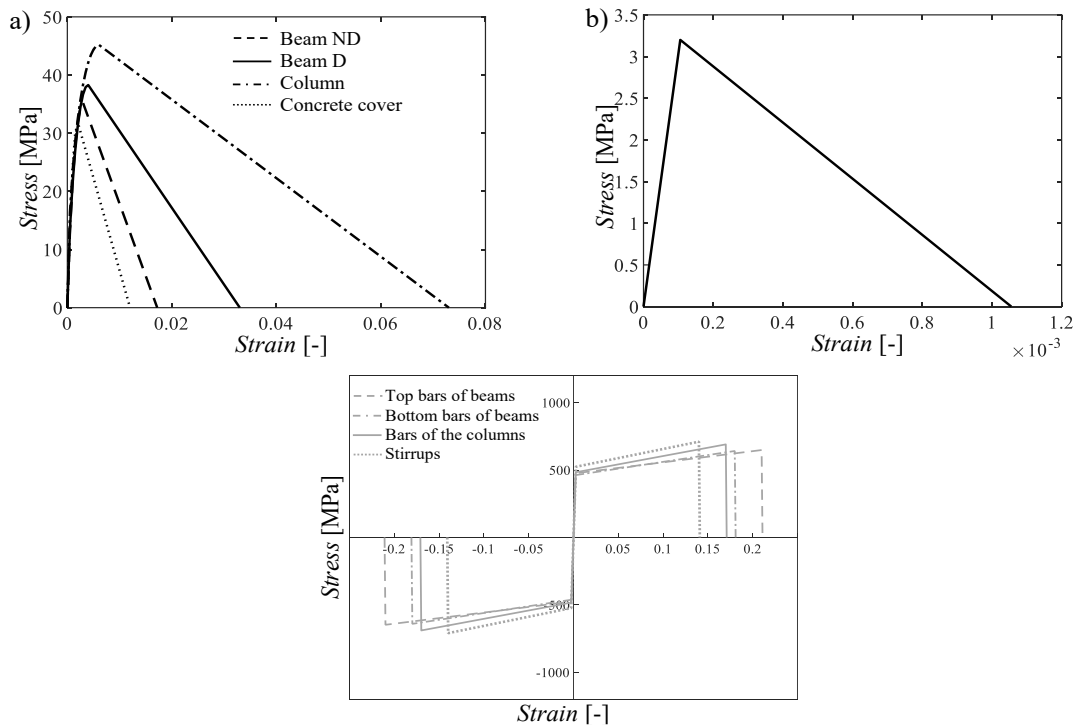

Fig. A3 Constitutive laws of materials assuming mean values of the mechanical properties for: a) concrete in compression; b) concrete in tension; c) steel bars in tension and in compression.

Concerning the concrete behaviour in compression (Fig. A3(a)), the behaviour before the peak stress

is derived by the formula in CEB-FIP Model Code 90 [40], while the post-peak response is described by a linearly descending branch and it is based on a local strain softening according to Saatcioglu and Razvi model [41], in order to account for the multiaxial state of stress due to the confinement of concrete in compression. In fact, the beams are subjected to compressive forces during the initial stages of the progressive collapse phenomena, which should be taken into account both in terms of resistance and ductility. The reduction of compressive strength due to cracks is taken equal to 0.45, representing the maximal strength reduction under large transverse strain, as suggested by [42] and in line with the experimental results of [43].

The tensile concrete behaviour (Fig. A3(b)) has been modelled choosing a local strain tension softening, accounting for the tension stiffening effect [44] through a linear post-peak branch up to the zero strength in correspondence of a strain equal to $10f_{ct}/E_c$, being f_{ct} the tensile strength of concrete and E_c the secant elastic modulus, computed according to [45]. Besides, the cracking process has been reproduced using the "Smeared cracking" with the fixed crack direction model [42],[46].

As for the reinforcement steel (Fig. A3(c)), a bi-linear constitutive law in tension and in compression has been adopted with hardening law. The reinforcement has been modelled with discrete bar elements assuming a perfect bond with the surrounding concrete. It should be noted that, buckling of reinforcement in the compressive zone is not considered since no buckling phenomena were declared during the experimental test. This derives also from the seismic design with a larger number of stirrups in the dissipative zones.

Within Atena 2D [39], the loading scheme consists in the application of the self-weight, followed by an imposed vertical displacement at a rate of 1 cm in correspondence of the loading point (i.e., top of the central column). In line with the experimental test, a steel plate of around 5 cm is placed on top of the central column. The solution of the equations is solved by adopting a standard Newton-Raphson iterative procedure considering 2500 maximum iterations and respecting contemporarily all the following four tolerance criteria [47]-[48]: 1.0% for the norm of displacement error; from 1.0% to 2.5% for the norm of residual force error; from 1.0% to 2.5% for the maximum error of residual forces; 1.0‰ for the out-of-balance energy error.

The comparison between the experimental and numerical capacity curves (Fig. A4(a)) and horizontal versus vertical displacements (Fig. A4(b)) is shown. It should be noted that not considering the concrete confinement effects implies an underestimation of both the resistance and ductility of the response with a fail in capturing the evolution of the horizontal displacements [31],[63].
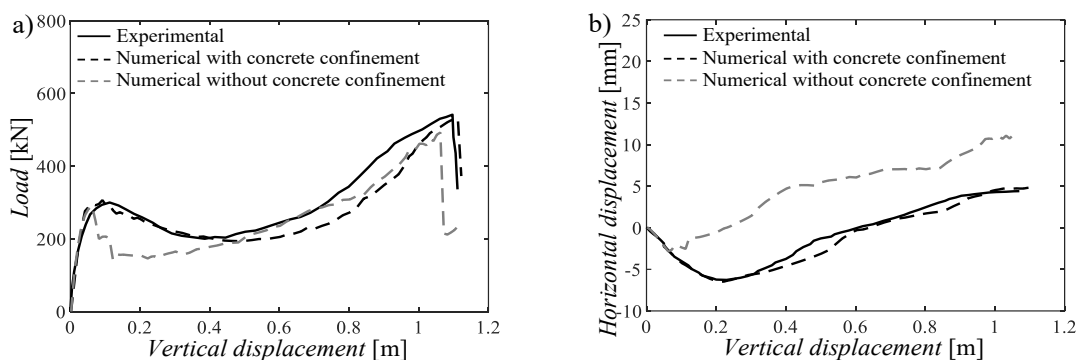

Fig. A4 Comparison between numerical and experimental response: a) capacity curve; b) horizontal displacement at the beam-column nodes.

APPENDIX B

In this appendix, the other numerical results related to the second, third and fourth failure scenarios are reported. In detail, the following figures show the capacity curves together with the horizontal and vertical displacements of the nodes corresponding to the different x- and y-direction frames
Fig. B1 shows the results related to second failure scenario for the frame FS2-x (i.e., x-direction).
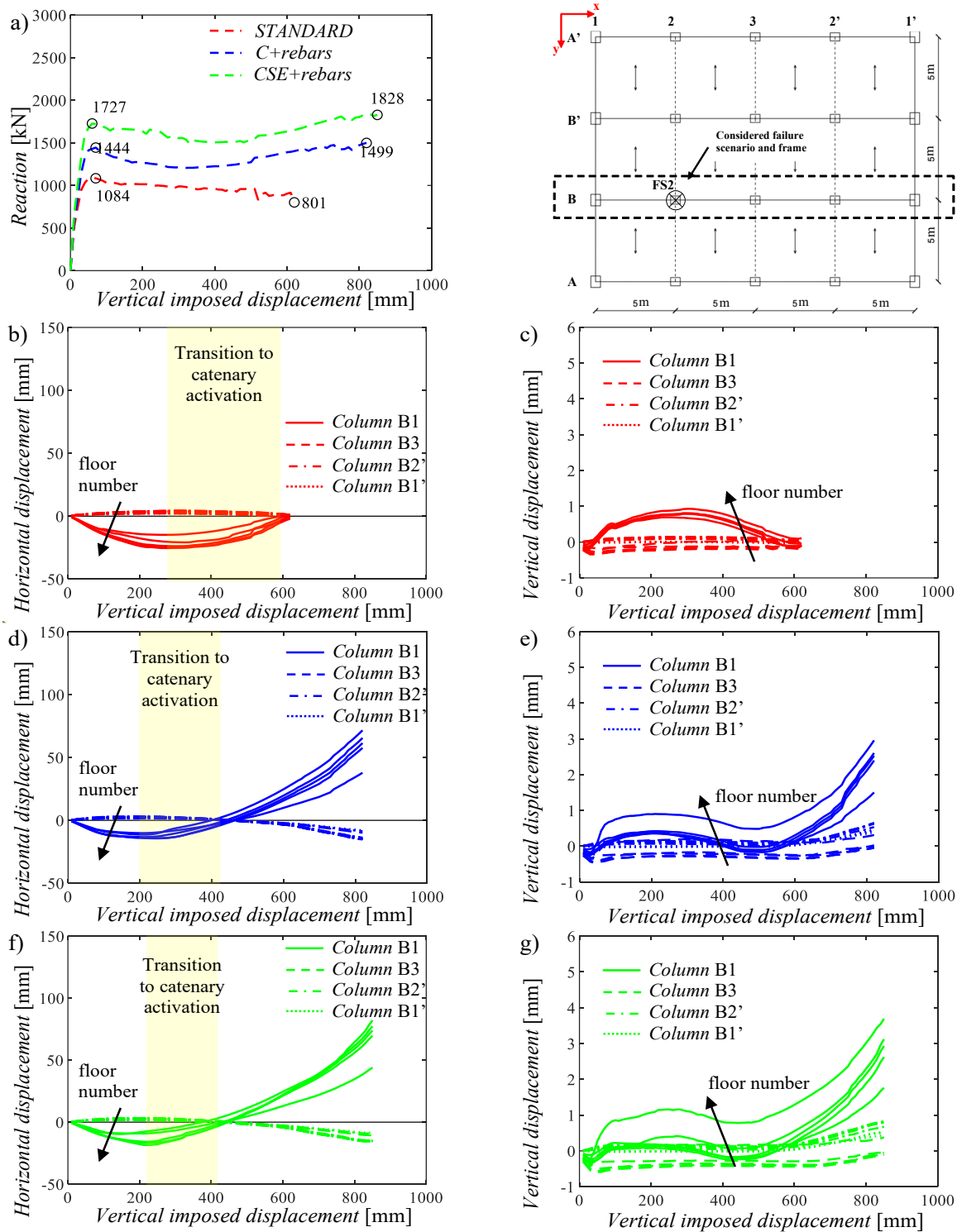

Fig. B1 Results of the displacement-controlled pushdown analyses of the frame FS2-x (i.e., second failure scenario – x-direction): (a) capacity curves; (b),(d),(f) horizontal displacements of the beam-column nodes for *STANDARD*, *C+rebars* and *CSE+rebars* configurations; (c),(e),(g) vertical displacements of the beam-column nodes for *STANDARD*, *C+rebars* and *CSE+rebars* configurations.

In Fig. B2, the results related to the second failure scenario for the frame FS2-y (i.e., y-direction) are shown.
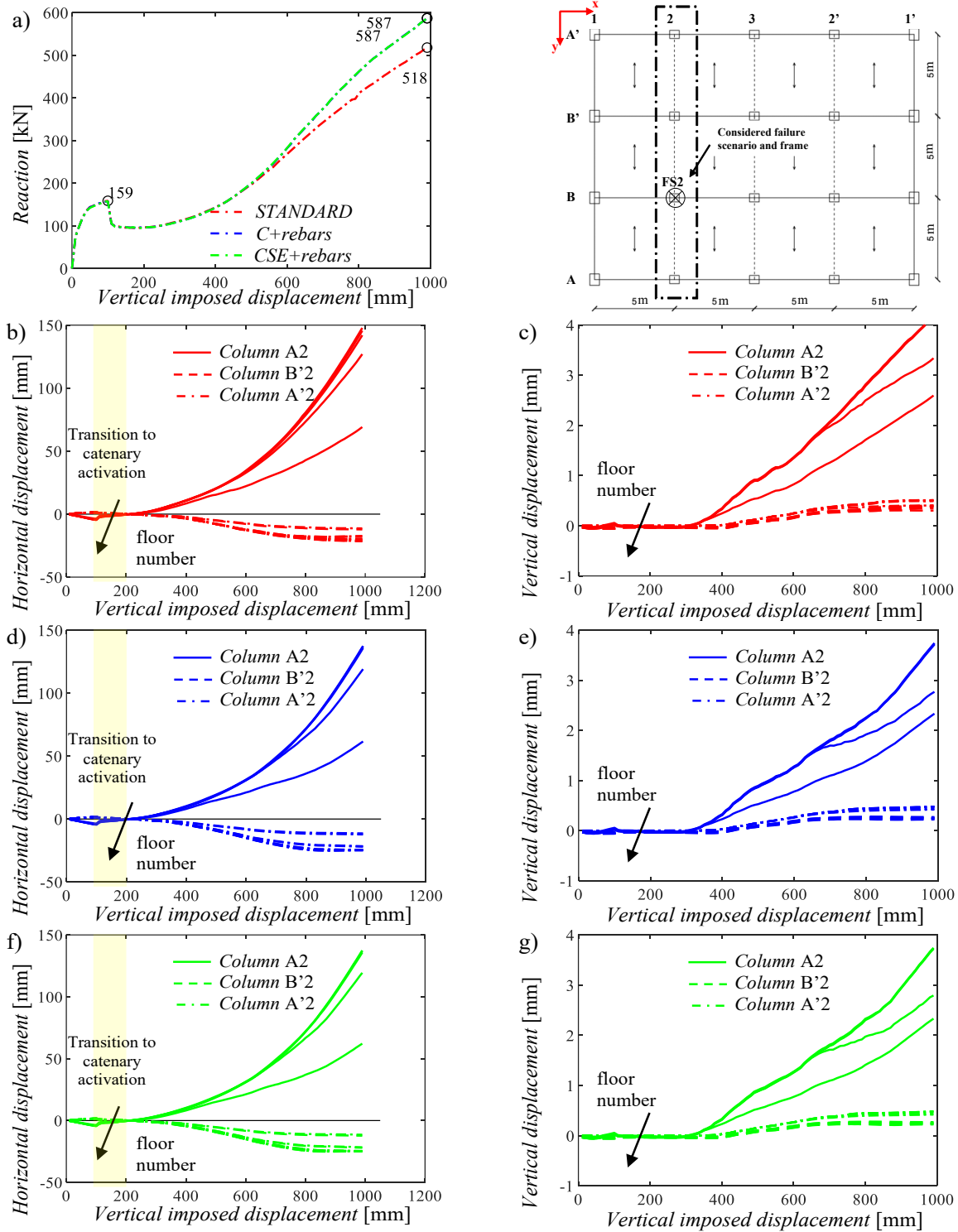

Fig. B2 Results of the displacement-controlled pushdown analyses of the frame FS2-y (i.e., second failure scenario – y-direction): (a) capacity curves; (b),(d),(f) horizontal displacements of the beam-column nodes for *STANDARD*, *C+rebars* and *CSE+rebars* configurations; (c),(e),(g) vertical displacements of the beam-column nodes for *STANDARD*, *C+rebars* and *CSE+rebars* configurations.

In Fig. B3, the outcomes corresponding to the third failure scenario for the frame FS3-x (i.e., x-direction) are shown.
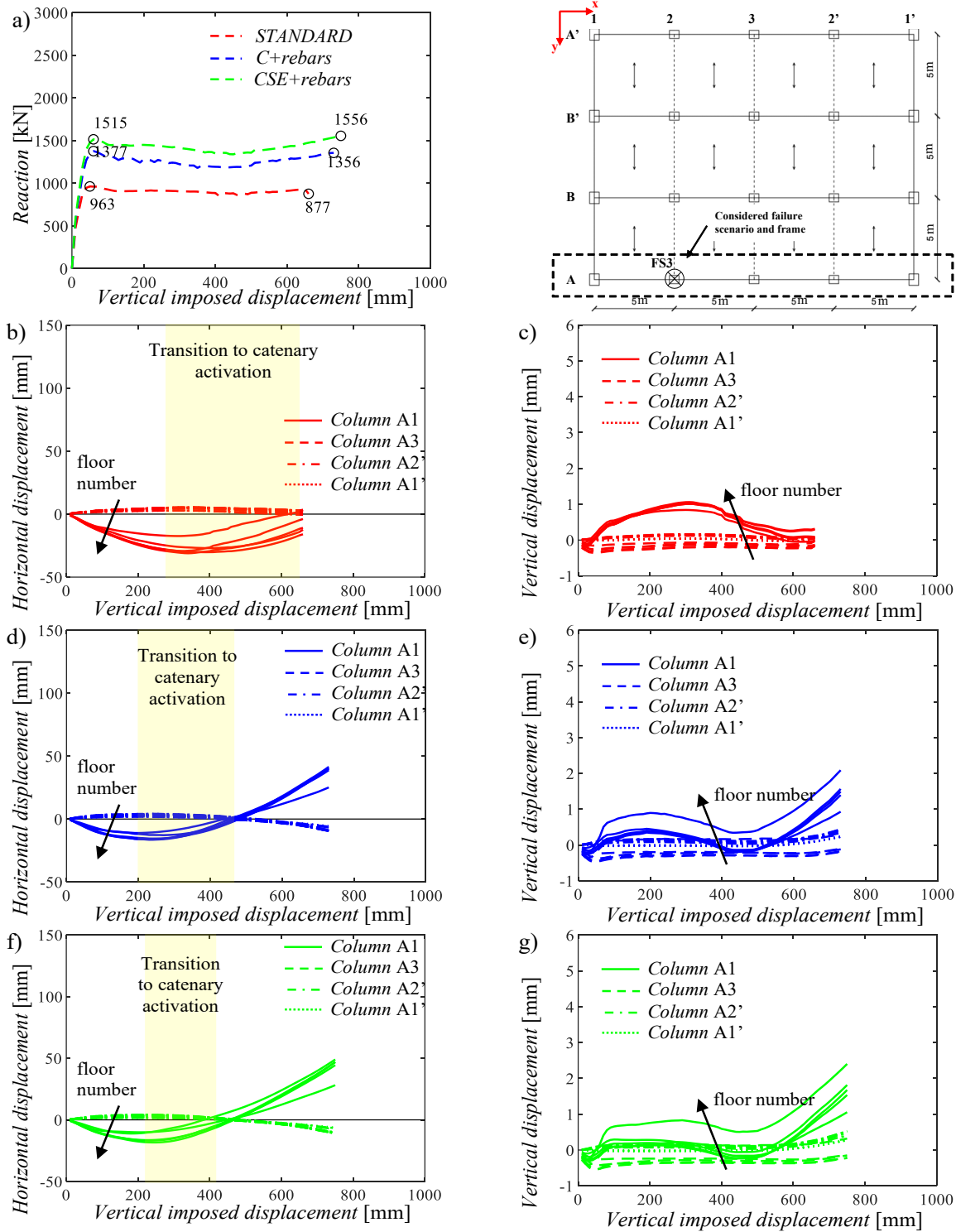

Fig. B3 Results of the displacement-controlled pushdown analyses of the frame FS3-x (i.e., third failure scenario – x-direction): (a) capacity curves; (b),(d),(f) horizontal displacements of the beam-column nodes for *STANDARD*, *C+rebars* and *CSE+rebars* configurations; (c),(e),(g) vertical displacements of the beam-column nodes for *STANDARD*, *C+rebars* and *CSE+rebars* configurations.

Fig. B4 depicts the resuls of the frame FS3-y (i.e., y-direction) for the third failure scenario.
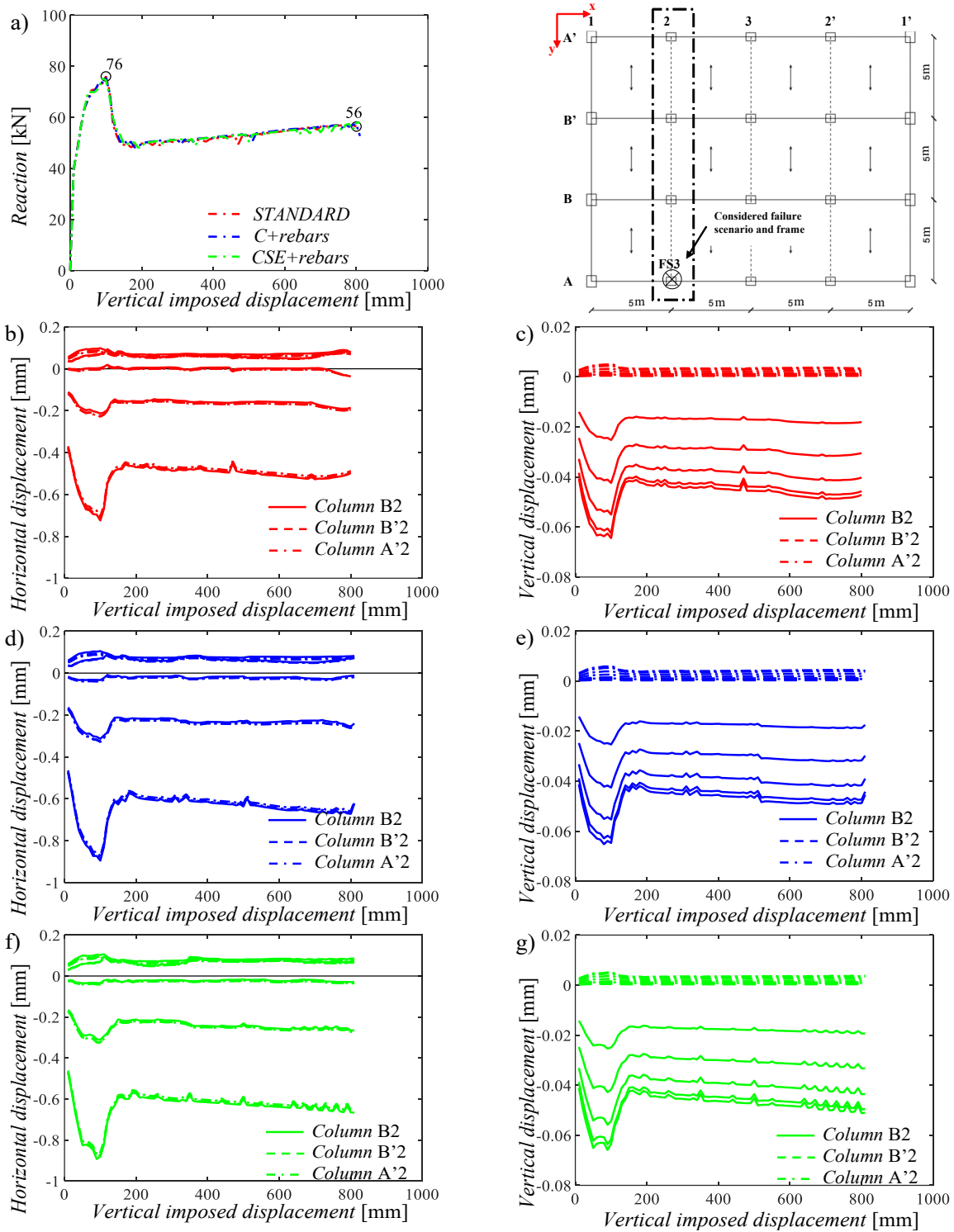

Fig. B4 Results of the displacement-controlled pushdown analyses of the frame FS3-y (i.e., third failure scenario – y-direction): (a) capacity curves; (b),(d),(f) horizontal displacements of the beam-column nodes for *STANDARD*, *C+rebars* and *CSE+rebars* configurations; (c),(e),(g) vertical displacements of the beam-column nodes for *STANDARD*, *C+rebars* and *CSE+rebars* configurations.

Fig. B5 illustrates the outcomes corresponding to the fourth failure scenario for the frame FS4-x (i.e., x-direction).
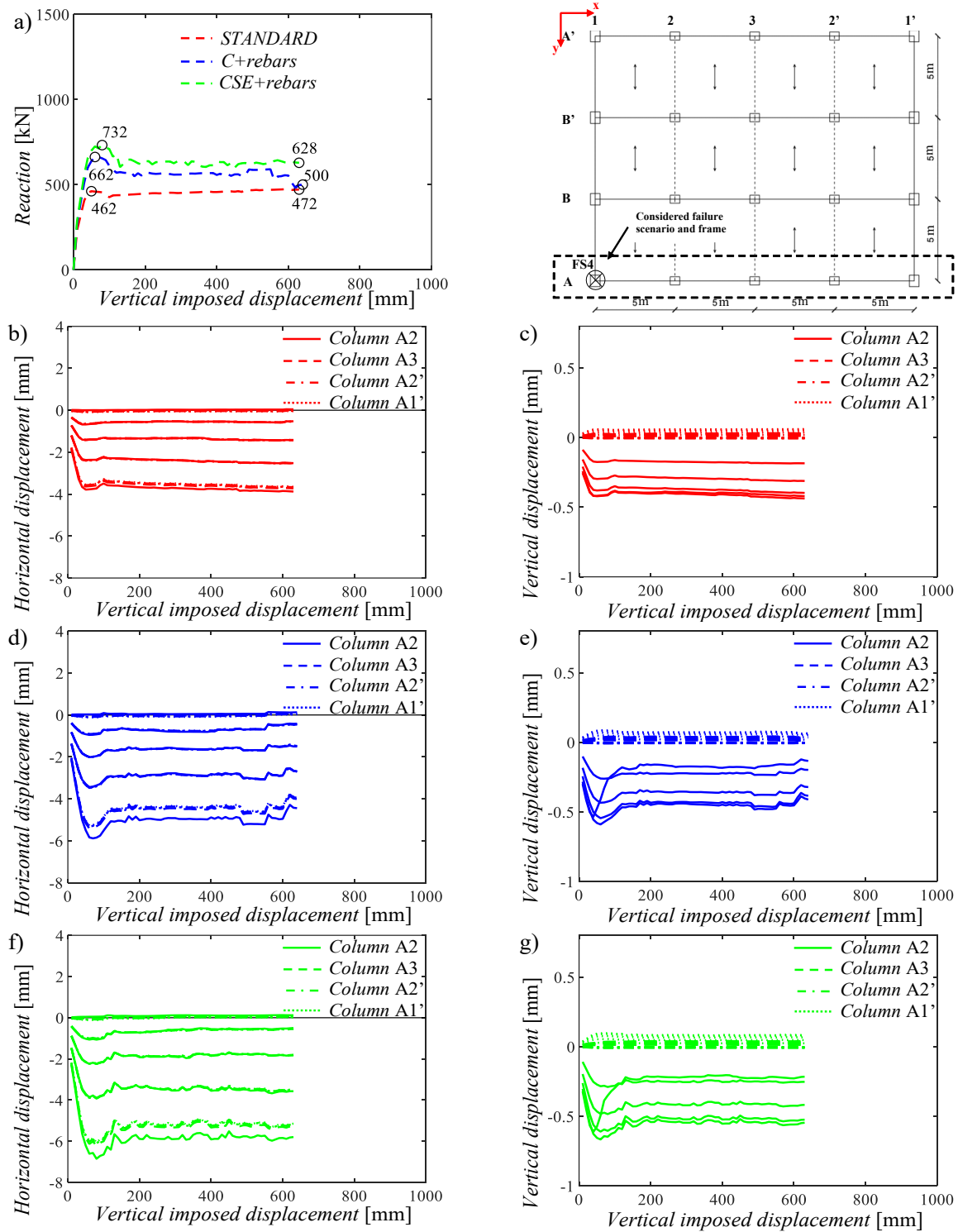

Fig. B5 Results of the displacement-controlled pushdown analyses of the frame FS4-x (i.e., fourth failure scenario – x-direction): (a) capacity curves; (b),(d),(f) horizontal displacements of the beam-column nodes for *STANDARD*, *C+rebars* and *CSE+rebars* configurations; (c),(e),(g) vertical displacements of the beam-column nodes for *STANDARD*, *C+rebars* and *CSE+rebars* configurations.

In Fig. B6, the results of the frame FS4-y (i.e., y-direction) for the fourth failure scenario are shown.
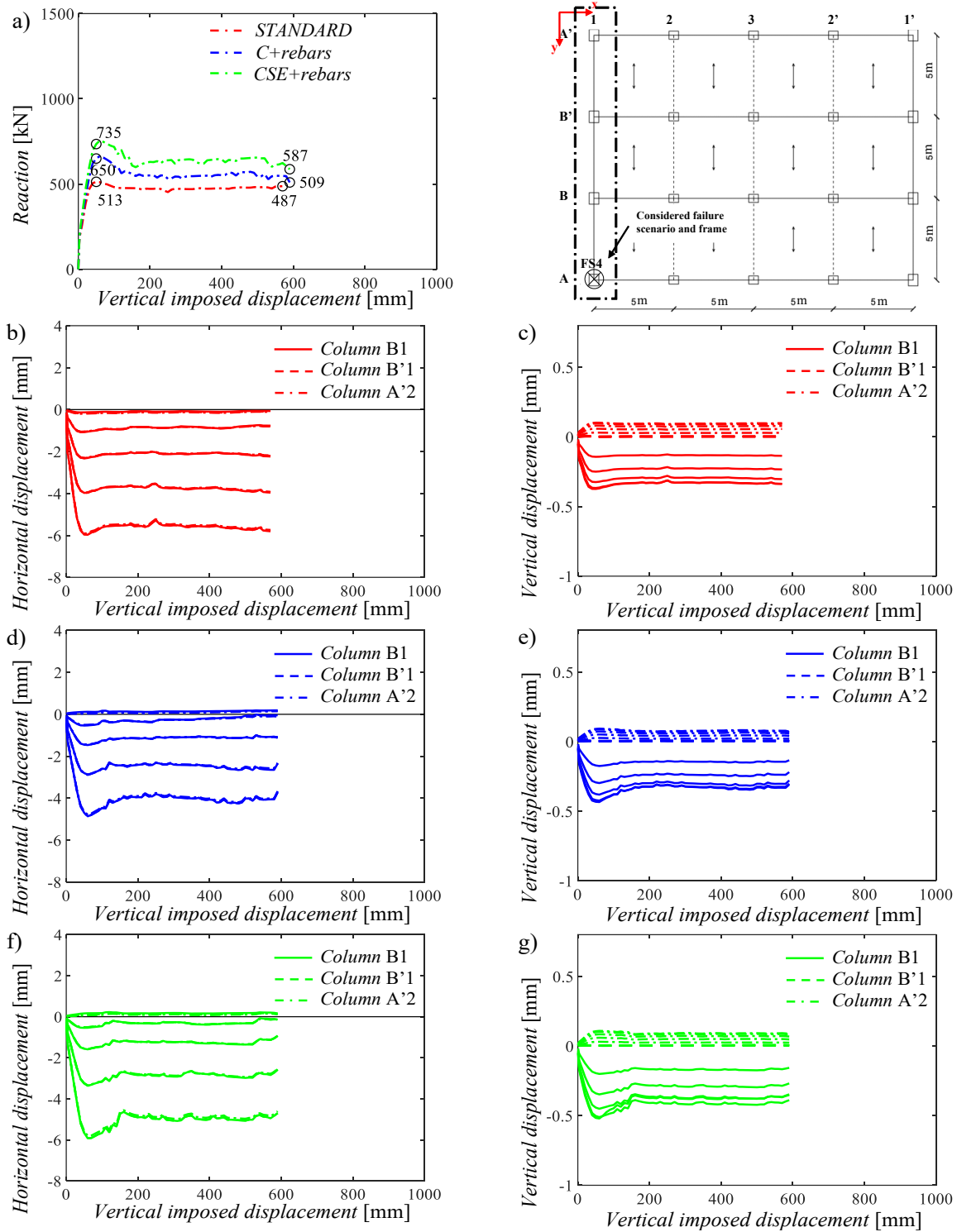

Fig. B6 Results of the displacement-controlled pushdown analyses of the frame FS4-y (i.e., fourth failure scenario – y-direction): (a) capacity curves; (b),(d),(f) horizontal displacements of the beam-column nodes for *STANDARD*, *C+rebars* and *CSE+rebars* configurations; (c),(e),(g) vertical displacements of the beam-column nodes for *STANDARD*, *C+rebars* and *CSE+rebars* configurations.

REFERENCES

[1] Ellingwood BR. Mitigating risk from abnormal loads and progressive collapse. J Perform Constr Facil 2006;20(4):315–23.

[2] Starossek U, Smilowitz R, Waggoner M, Rubenacker K J, Haberland, M. Report of the terminology and procedures sub-committee (SC1): recommendations for design against disproportionate collapse of structures. In: ASCE SEI 2011 structures congress. Las Vegas; 2011.

[3] CEN Comité Européen de Normalisation. EN 1991-1-7: Eurocode 1 – actions on structures – part 1–7: general actions – accidental actions. Brussels (Belgium): CEN; 2006.

[4] Department of Communities and Local Government. The building regulations 2010 - structure: approved document A. UK: HM Government; 2010.

[5] Department of Defence (DoD). Design of buildings to resist progressive collapse (UFC 4-023-03). Washington, DC: Unified Facilities Criteria; 2009.

[6] American Society of Civil Engineers (ASCE). Minimum design loads and associated criteria for buildings and other structures (ASCE/SEI 7-16), 2016.

[7] General Services Administration (GSA). Alternative path analysis and design guidelines for progressive collapse resistance. Washington, DC: Office of Chief Architects; 2013.

[8] Droogné, D., Botte, W., & Caspeele, R. (2018). A multilevel calculation scheme for risk-based robustness quantification of reinforced concrete frames. *Engineering Structures*, *160*, 56–70. https://doi.org/10.1016/j.engstruct.2017.12.052

[9] Botte, W., Gouverneur, D., Caspeele, R., & Taerwe, L. (2015). Influence of Design Parameters on Tensile Membrane Action in Reinforced Concrete Slabs. *Structural Engineering International : Journal of the International Association for Bridge and Structural Engineering (IABSE)*, *25*(1), 50–60. https://doi.org/10.2749/101686614X14043795570174

[10] M. Scalvenzi, S. Gargiulo, F. Freddi, F. Parisi, Impact of seismic retrofitting on progressive collapse resistance of RC frame structures, Eng. Fail. Anal. 131 (2022), 105840.

[11] Belletti, B., Damoni, C., Cervenka, V., & Hendriks, M. A. N. (2016). Catenary action effects on the structural robustness assessment of RC slab strips subjected to shear and tensile forces. *Structural Concrete : Journal of the FIB*, *17*(6), 1003–1016.

[12] Belletti B, Muttoni A, Ravasini S, Vecchi F. Parametric analysis on punching shear resistance of reinforced concrete continuous slabs. Magazine of Concrete Res. 2018;71(20):1083-1096.

[13] Guice LK, Rhomberg EJ. Membrane action in partially restrained slabs. ACI Struct J 1988;85.

[14] Park R. Tensile membrane behaviour of uniformly loaded rectangular reinforced concrete slabs with fully restrained edges. Mag Concr Res 1964;16:39–44. http://dx.doi.org/10.1680/macr.1964.16.46.39.

[15] Vecchio FJ, Tang K. Membrane action in reinforced concrete slabs. Can J Civ Eng 1990;17:686–97. http://dx.doi.org/10.1139/l90-082.

[16] Pham AT, Tan KH. A simplified model of catenary action in reinforced concrete frames under axially restrained conditions. Magazine of Concrete Research 2017;1700009.

[17] Fascetti A, Kunnath SK, Nisticò N. Robustness evaluation of RC frame buildings to progressive collapse. Engineering Structures 2015;86:242-249.

[18] Brunesi E, Parisi F. Progressive collapse fragility models of European reinforced concrete framed buildings based on pushdown analysis. Engineering structures 2017;152:579–596.

[19] Ying Wang, Bin Zhang, Xiang-Lin Gu, Feng Lin, Experimental and numerical investigation on progressive collapse resistance of RC frame structures considering transverse beam and slab effects, Journal of Building Engineering, Volume 47, 2022, 103908, ISSN 2352-7102.

[20] Mengxue Guo, Hua Huang, Shilin Yang, Min Huang, Experimental and numerical investigation on progressive collapse resistance of three-dimensional RC structures, Eng. Fail. Anal. 167, 108954 (2025).

[21] K. Qian, B. Li, Z.W. Zhang Testing and simulation of 3D effects on progressive collapse

resisting of RC buildings Mag. Concr. Res., 66 (3–4) (2014), pp. 163-178.

[22] Li H and El-Tawil S(2011) Three-dimensional effects inprogressive collapse modeling.Proceedings of the StructuresCongress 2011, pp. 2829–2839, http://dx.doi.org/10.1061/41171(401)246.

[23] MIT, Istruzioni per l'applicazione dell'«Aggiornamento delle "Norme tecniche per le costruzioni"» di cui al decreto ministeriale 17 gennaio 2018, 2019.

[24] European Committee for Standardization, Eurocode 8 – Design of Structures for earthquake resistance, 1998.

[25] Miceli, E., & Castaldo, P. (2024). Robustness improvements for 2D reinforced concrete moment resisting frames: Parametric study by means of NLFE analyses. *Structural Concrete: Journal of the FIB*, *25*(1), 9–31. https://doi.org/10.1002/suco.202300443

[26] E. Miceli, D. Gino, P. Castaldo (2025): Reliability assessment of robustness for reinforced concrete moment resisting frames - Developments in the Built Environment, 100639 (DOI: https://doi.org/10.1016/j.dibe.2025.100639)

[27] Izzuddin BA, Vlassis AG, Elghazouli AY, Nethercot DA. Progressive collapse of multi-storey buildings due to sudden column loss - Part I: Simplified assessment framework. Engineering Structures 2008;30(5):1308–1318.

[28] Ren P, Li Y, Lu X, Guan H, Zhou Y. Experimental Investigation of Progressive Collapse Resistance of One-way Reinforced Concrete Beam–slab Substructures under a Middle-column-removal Scenario. Engineering Structures 2016;118:28-40.

[29] Lu X, Lin K, Li Y, Guan H, Ren P, Zhou Y. Experimental Investigation of RC Beam-slab Substructures against Progressive Collapse Subject to an Edge-column-removal Scenario 2017. Engineering Structures;149:91-103.

[30] Zhang L, Zhao H, Wang T, Chen Q. Parametric Analysis on Collapse-resistance Performance of Reinforced-concrete Frame with Specially Shaped Columns Under Loss of a Corner Column. The Open Construction and Building Technology Journal 2016;10(1):466-480.

[31] Lew HS, Bao Y, Sadek F, Main JA, Pujol S, Sozen, MA. An experimental and computational study of reinforced concrete assemblies under a column removal scenario. NIST Technical Note 2011;1720(106).

[32] Brunesi E, Nascimbene R, Parisi F, Augenti N. Progressive Collapse Fragility of Reinforced Concrete Framed Structures through Incremental Dynamic Analysis. Engineering Structures 2015;104:65-79.

[33] Consiglio Nazionale delle Ricerche, Istruzioni per la valutazione della robustezza delle costruzioni, 2018.

[34] Hussein M. Elsanadedy, Aref A. Abadel, High-fidelity FE models for assessing progressive collapse robustness of RC ordinary moment frame (OMF) buildings, Engineering Failure Analysis 136, 106228 (2022).

[35] Adam JM, Buitrago M, Bertolesi E, Sagaseta J, Moragues JJ. Dynamic Performance of a Real-scale Reinforced Concrete Building Test under a Corner-column Failure Scenario. Engineering Structures 2020;210:110414.

[36] Cantone R, Belletti B, Manelli L, Muttoni A. Compressive membrane action effects on punching strength of flat RC slabs. Key Engineering Materials 2016;711:698-705.

[37] Di Trapani F, Giordano L, Mancini G. Progressive Collapse Response of Reinforced Concrete Frame Structures with Masonry Infills. Journal of Engineering Mechanics 2020;146-3.

[38] CSI, SAP2000 Integrated software for structural analysis and Design, Computers and Structures Inc., Berkley, California.

[39] Cervenka Consulting s.r.o., ATENA 2D v5, Prague, Czech Republic, 2014.

[40] CEB-FIP Model Code 1990, First Draft, Comittee Euro-International du Beton, Bulletin d'information No. 195,196, Mars.

[41] M. Saatcioglu and S.R.Razvi, "Strength and ductility of confined concrete", J. Struct. Eng. (United States), vol. 119, no. 10, pp. 3109-3110, 1993.

[42] Vladimír Červenka, Libor Jendele, and Jan Červenka. ATENA Program Documentation Part 1 Theory. Ed. by Cervenka Consulting Ltd. 2012.

[43] Dyngeland, T. (1989) - Behavior of Reinforced Concrete Panels, Dissertation, Trondheim University, Norway, BK-report 1989:1.

[44] Massicotte B, Elwi AE, MacGregor JG. "Tension-stiffening models for planar reinforced concrete members". Journal of Structural Engineering 116(11):3039–58, 1990.

[45] European Committee for Standardization, Eurocode - Basis of structural and geotechnical design, 1990.

[46] Darwin, D., Pecknold, D.A.W. (1974). Inelastic Model for Cyclic Biaxial Loading of Reinforced Concrete. Civil Engineering Studies, University of Illinois, July.

[47] Max A.N. Hendriks and Marco A. Roosen (editors), "Guidelines for Nonlinear Finite Element Analysis of Concrete Structures", Rijkswaterstaat Centre for Infrastructure, Report RTD:1016-1:2019, 2019.

[48] Gino D., Miceli E., Castaldo P., Recupero A., Mancini G. "Strain-based method for assessment of global resistance safety factors for NLNAs of reinforced concrete structures", Engineering Structures, 2024, 117625, https://doi.org/10.1016/j.engstruct.2024.117625.

[49] Lim NS, Tan KH, Lee CK. Effects of rotational capacity and horizontal restraint on development of catenary action in 2-D RC frames. Engeneering Structures 2017;153:613–27.

[50] Yu J, Tan KH. Structural behavior of RC beam-column subassemblages under a middle column removal scenario. Journal of Structural Engineering 2013;139(2):233–50.

[51] Yu J, Tan KH. Experimental and numerical investigation on progressive collapse resistance of reinforced concrete beam column sub-assemblages. Engineering Structures 2013;55:90–106.

[52] Qian K, Li B, Ma JX. Load-carrying mechanism to resist progressive collapse of RC buildings. Journal of Structural Engineering 2015;141(2):1–14.

[53] Xuan DP, Tan KH. Experimental study of beam-slab substructures subjected to a penultimate-internal column loss. Engineering Structures 2013;55:2–15.

[54] Zheng Tan, Wei-hui Zhong, Bao Meng, Yu-hui Zheng, Shi-chao Duan, Effect of various boundary constraints on the collapse behavior of multi-story composite frames, Journal of Building Engineering, Volume 52, 2022, 104412, https://doi.org/10.1016/j.jobe.2022.104412.

[55] American Society of Civil Engineers (ASCE) for the Federal Emergency Management Agency. Pre-standard and commentary for the seismic rehabilitation of buildings, FEMA Report 356. Washington, DC; 2000.

[56] Panagiotakos, Telemachos B. and Michael N. Fardis. "Deformations of Reinforced Concrete Members at Yielding and Ultimate." Aci Structural Journal 98 (2001): 135-148.

[57] Castaldo P, Gino D, Mancini G. Safety formats for non-linear finite element analysis of reinforced concrete structures: discussion, comparison and proposals. Eng Struct. 2019;193:136–53. https://doi.org/10.1016/j.engstruct.2019.05.029

[58] Gino, D., Castaldo, P., Giordano, L., Mancini, G., Model uncertainty in non-linear numerical analyses of slender reinforced concrete members, Structural Concrete, 2021, 22(2), 845–870.

[59] Castaldo P, Gino D, Carbone VI, Mancini G, Framework for definition of design formulations from empirical and semi-empirical resistance models, Structural Concrete, 2018, 19(4), 980–987.

[60] Castaldo, P., Gino, D., Bertagnoli, G., Mancini, G. Partial safety factor for resistance model uncertainties in 2D non-linear finite element analysis of reinforced concrete structures, Engineering Structures, 2018, 176, pp. 746–762.

[61] Giacomo Caredda, Nirvan Makoond, Manuel Buitrag, Juan Sagaseta, Marios Chryssanthopoulos, Jose M. Adam, Enhancing building robustness through a fuse-based, Developments in the Built Environment segmentation framework 19, 100515, 2024.

[62] American Concrete Institute (ACI). "Building Code Requirements for Structural Concrete (ACI 318-02)". Washington, DC, 2002.

[63] Miceli E, Ferrara S, Castaldo P, Confinement effects within the seismic design of reinforced concrete frames: reliability assessment and comparison, Engineering Structures 313, 118248, 2024 10.1016/j.engstruct.2024.118248.